with iatrogenic, congenital, or acquired immunodeficiency can reveal an increased number of EBV-infected cells in the lymph nodes.[4] EBV is also associated with various malignant lymphomas and lymphoproliferative disorders.

Only 1 case of IgG4-related lymphadenopathy with EBV-infected cells has been reported, and the relationship between IgG4-related disease and EBV has not been fully addressed.[5] Hence, we analyzed the association of EBV and IgG4-related disease. Lymph node tissues from subjects with various morphologic types of IgG4-related lymphadenopathy were subjected to EBER in situ hybridization (ISH) to examine the presence and localization of EBER$^+$ cells. For comparison with extranodal lesions, IgG4-related lacrimal gland disease, IgG4-related submandibular gland disease, IgG4-related skin disease, and IgG4-related pancreatitis were also examined. Non–IgG4-related benign lymph node hyperplasia and lymph nodes of AITL were also examined for comparison.

MATERIALS AND METHODS

Patients and Materials

Thirty-one Japanese patients with IgG4-related lymphadenopathy, 9 with IgG4-related lacrimal gland disease, 10 with IgG4-related submandibular disease, 2 with IgG4-related skin disease, 3 with IgG4-related pancreatitis, 22 with IgG4$^-$ reactive lymphoid hyperplasia, and 10 with AITL were included. All cases were retrieved from the surgical pathology consultation files of the Department of Pathology, Graduate School of Medicine, Dentistry, and Pharmaceutical Sciences, Okayama University in Okayama, Japan.

The diagnoses of IgG4-related disease were based upon the consensus statement on the pathology of IgG4-related disease published in 2012.[6] The clinical records and pathology materials of all IgG4-related diseases were reviewed, and cases of multicentric Castleman disease, malignant lymphoma, or other lymphoproliferative disorders (including rheumatoid arthritis–related lymphadenopathy and other immune-mediated conditions) were excluded. The number of IgG4$^+$ cells in the cases of IgG4-related lymphadenopathy ranged from 122 to 477 per high-power field (HPF) (mean ± SD, 250 ± 102). The ratio of IgG4$^+$/IgG$^+$ cells was >0.4 in all cases. The specimens of IgG4-related lymphadenopathy were reviewed by the authors Y.S. and M.T. and morphologically categorized into the following subtypes as previously reported[1,7]: Castleman disease–like morphology (type I); reactive follicular hyperplasia (type II); interfollicular expansion and increased immunoblasts (type III); PTGC-type (type IV); and inflammatory pseudotumor-like morphology (type V).

In sections of IgG4-related lacrimal gland disease, IgG4-related submandibular gland disease, IgG4-related skin disease, and IgG4-related pancreatitis, characteristic morphologic features and increased IgG4$^+$ cells were seen. Only in cases of IgG4-related skin diseases, the required numbers of IgG4$^+$ plasma cells were not seen; however, in a previous study of IgG4-related skin disease, we suggested that the cutoff of 200 IgG4$^+$ plasma cells/HPF appeared to be controversial.[8] Two patients with IgG4-related lacrimal gland disease (cases Ex4 and Ex7) were the same patients with IgG4-related lymphadenopathy listed in Table 1 (cases LN6 and LN25, respectively).

To examine whether increased numbers of EBV-infected cells in benign lymph nodes was specifically associated with IgG4-related disease rather than other patient characteristics, EBER detection by ISH was also performed on 22 lymph nodes with IgG4$^-$ lymphoid hyperplasia. The cases of reactive lymphoid hyperplasia did not suggest Castleman disease or any other distinct lymphoproliferative diseases and also did not meet the histologic diagnostic criteria for IgG4-related disease.

To compare with type III IgG4-related lymphadenopathy, immunostaining for IgG4 was performed in 10 lymph nodes with AITL. Cases of AITL were diagnosed on the basis of *World Health Organization (WHO) Classification of Tumours of Haematopoietic and Lymphoid Tissues* (fourth edition).[9] All cases showed typical histologic features including infiltration of small to medium-sized T cells with clear cytoplasm and proliferation of high endothelial venules. Many EBER$^+$ B cells (from 23 to >1000/0.5 cm^2; mean ± SD 422 ± 399) were observed in 8 of 10 cases (80%), which is similar to the percentage described in the WHO monograph (75%).[9]

Histologic Examination and Immunohistochemistry

Surgically biopsied lymph node specimens were fixed in 10% formaldehyde and embedded in paraffin. Serial sections (4 μm) were cut from each paraffin-embedded tissue block, and stained with hematoxylin and eosin. An automated Bond Max stainer (Leica Biosystems, Melbourne, Vic., Australia) was used for immunohistochemistry. The tissue sections were subjected to standard heating or enzymatic pretreatment for antigen retrieval. The following primary antibodies were used: IgG (polyclonal; 1:20,000; Dako, Carpinteria, CA), IgG4 (HP6025; 1:400; The Binding Site, Birmingham, UK), FOXP3 (236A/E7; 1:100; Abcam, Cambridge, UK), and latent membrane protein-1 (LMP-1) (CS1-CS4; 1:10; Novocastra).

On the basis of the consensus statement on the pathology of IgG4-related disease,[6] 3 different HPFs (eyepiece, ×10; lens, ×40) were examined to calculate the average number of IgG4$^+$ cells per HPF and the IgG4$^+$/IgG$^+$ cell ratio. FOXP3$^+$ cells were also counted at 3 different HPFs with the highest density to calculate the average numbers per HPF.

In Situ Hybridization

ISH of EBER was performed using an automated Bond Max stainer (Leica Biosystems). Three representative fields per case were captured using a ×4 objective lens (covering 0.167 cm^2) to count EBER$^+$ cells per 0.5 cm^2. Increased numbers of EBV$^+$ cells was defined as >10 EBER$^+$ cells/0.5 cm^2.[10] EBER-ISH$^+$ and LMP-1$^-$ cases were classified into EBV latency type I.

© 2014 Lippincott Williams & Wilkins

Copyright © Lippincott Williams & Wilkins. Unauthorized reproduction of this article is prohibited.

TABLE 1. Clinical Features of 31 Patients of IgG4-related Lymphadenopathy

No.	Age/Sex	Affected Lymph Nodes	Extranodal Sites	IgG4 (mg/dL; nl = 4.8-105)	IgG (mg/dL)	IgG4/IgG (%; nl = 3-6)
LN1	58/M	Cervix, supraclavicle, axilla, mediastinum, porta hepatis, lesser omentum		2010	3536	57
LN2	74/M	Cervix, para-aorta, parailiac artery	Submandibular gland	NA	4050	NA
LN3	59/M	Cervix, supraclavicle, axilla, mediastinum, inguen		1140	5257	22
LN4	64/F	Left cervix, mediastinum		446	1989	22
LN5	82/F	Right auricular, supraclavicle	Salivary gland	327	1094	30
LN6*	36/F	Cervix, supraclavicle	Lacrimal gland	561	1961	29
LN7	64/M	Mediastinum, axilla	Right lung	641	3134	20
LN8	77/M	Systemic		1100	5800	19
LN9	78/M	Mediastinum, axilla, inguen		1090	5174	21
LN10	82/M	Cervix, inguen, para-aorta, mediastinum	Parotid gland, lacrimal gland	1050	3447	30
LN11	68/F	Axilla, mediastinum, abdomen, inguen		2120	5057	42
LN12	67/M	Cervix, mediastinum, axilla, para-aorta		583	2468	24
LN13	76/M	Cervix, axilla, para-aorta, inguen		1040	3930	26
LN14	59/F	Supraclavicle, mediastinum, abdomen, inguen	Lacrimal gland, submandibular gland	1500	2524	59
LN15	73/M	Abdomen, inguen	Kidney	505	1600	32
LN16	36/M	Left submandibulla		110	551	20
LN17	69/M	Right submandibulla		693	2315	30
LN18	71/M	Left submandibulla, submentum		275	2144	13
LN19	50/M	Bilateral submandibulla, cervix		183	2719	7
LN20	61/M	Systemic	Skin	1120	3025	37
LN21	51/F	Right submandibulla	Bilateral eyelid, parotid gland	223	NA	NA
LN22	70/M	Cervix	Bilateral parotid gland, right submandibular gland, pancreas	483	1190	41
LN23	67/M	Left submandibulla	Left submandibular gland	141	1543	9
LN24	67/M	Submandibulla	Right lung	389	1619	24
LN25†	68/M	Bilateral submandibulla	Bilateral lacrimal glands	1340	3090	43
LN26	63/M	Left submandibulla	Submandibular gland, kidney, mediastinum, aorta	2240	3007	74
LN27	65M	Right submandibulla, mediastinum	Bilateral lacrimal glands, submandibular gland, parotid gland, kidney	2550	6024	42
LN28	70M		Lung	236	1466	16
LN29	51F	Right submandibulla	Submandibular gland	NA	NA	NA
LN30	76M	Right submandibulla	Lacrimal gland, skin	NA	NA	NA
LN31	49M	Left submandibulla, cervix	Left submandibular gland	NA	NA	NA

*The same patient had IgG4-related lacrimal gland disease listed in Table 4 (Ex4).
†The same patient had IgG4-related lacrimal gland disease listed in Table 4 (Ex7).
F indicates female; LN, lymph node; M, male; NA; not available; nl; normal.

Polymerase Chain Reaction for Immunoglobulin Heavy Chain and T-cell Receptor γ Chain

DNA was extracted from formalin-fixed and paraffin-embedded tissues. T-cell receptor γ chain (TCRG) VgIf and Vg10 primers (tube A) and TCRG Vg9 and Vg11 primers (tube B) were used for TCR gene rearrangement study, and each of the tubes (A and B) also included 2 primers targeting the J segments (Jg1.1/2.1 and Jg1.3/Jg2.3) as previously reported.[11] Polymerase chain reaction (PCR) for immunoglobulin heavy chain (IgH) was also performed using consensus primers directed to VH framework (FR) II of the IgH gene using BIOMED-2 primer sets as previously described.[11] The products of PCR reactions were subsequently analyzed by ABI PRISM 310 Genetic Analyzer and Gene Mapper software version 3.7 (Applied Biosystems, CA).[12]

Statistical Analysis

Differences between groups were determined by the Student t test and χ^2 test with SPSS software (version 14.0; SPSS Inc., Chicago, IL). Values of $P < 0.05$ was considered to be statistically significant.

RESULTS

IgG4-related Lymphadenopathy

The clinical and pathologic findings for 31 cases of IgG4-related lymphadenopathy are summarized

© 2014 Lippincott Williams & Wilkins

Copyright © Lippincott Williams & Wilkins. Unauthorized reproduction of this article is prohibited.

TABLE 2. Pathologic Features of 31 Patients of IgG4-related Lymphadenopathy

No.	Histologic Subtype	EBER-ISH$^+$ Cells (/0.5 cm^2)	Distribution of EBER$^+$ Cells
LN1	Type I	0	
LN2	Type I	48	Interfollicular/scattered
LN3	Type I	27	Interfollicular/scattered
LN4	Type II	0	
LN5	Type II	3	
LN6	Type II	13	Interfollicular/scattered
LN7	Type II	25	Interfollicular/scattered
LN8	Type III	3	
LN9	Type III	0	
LN10	Type III	0	
LN11	Type III	163	Interfollicular/scattered
LN12	Type III	> 1000	Diffuse
LN13	Type III	> 1000	Diffuse
LN14	Type III	133	Interfollicular/scattered
LN15	Type III	52	Interfollicular/scattered
LN16	Type IV	0	
LN17	Type IV	1	
LN18	Type IV	0	
LN19	Type IV	9	
LN20	Type IV	10	
LN21	Type IV	6	
LN22	Type IV	6	
LN23	Type IV	19	Interfollicular/scattered
LN24	Type IV	12	Interfollicular/scattered
LN25	Type IV	248	Intrafollicular/localized
LN26	Type IV	72	Interfollicular/scattered
LN27	Type IV	46	Interfollicular/scattered
LN28	Type IV	27	Interfollicular/scattered
LN29	Type IV	20	Interfollicular/scattered
LN30	Type IV	55	Interfollicular/scattered
LN31	Type IV	27	Interfollicular/scattered

in Tables 1 and 2. There were 24 men and 7 women. The ages ranged from 36 to 82 years (mean ± SD, 64.5 ± 11.6). No patient had a record of congenital, iatrogenic, or acquired immunodeficiency. There was no evidence of acute infection of EBV, and EBV serology indicated past infection in all patients tested. Serum IgG4 levels were elevated in all 27 examined patients and ranged from 110 to 2550 mg/dL (mean ± SD, 869.0 ± 695.3). Twenty-seven patients had systemic or multifocal lymphadenopathy, whereas 4 cases of PTGC-type (type IV) IgG4-related lymphadenopathy were localized in the submandibular lymph nodes (cases LN16 to LN19).

Histologically, cases were classified into type I (n = 3), type II (n = 4), type III (n = 8), and type IV (n = 16) lymphadenopathy. The immunohistochemical and ISH findings are summarized in Table 3. Immunohistochemistry revealed numerous IgG4$^+$ cells ranging from 122 to 477/HPF (mean ± SD, 250 ± 102), and ratios of IgG4$^+$/IgG$^+$ cells were >0.4 in all cases. Greater than 10 EBER$^+$ cells/0.5 cm^2 were found in 18 of 31 cases (58%) with no significant differences in the rates of positivity between the 4 subgroups (2/3 type I, 2/4 type II, 5/8 type III, 9/16 type IV). EBER latency was classified into latency I in examined EBER$^+$ cases (LN12 and LN13). In 15 of 18 cases, scattered EBER$^+$ lymphocytes were seen in interfollicular areas. Two type III cases (cases LN12 and LN13) had numerous diffusely distributed EBER$^+$ cells, with some in intrafollicular areas as well (Fig. 1). EBER$^+$ cells included small lymphocytes and immunoblasts, as is found in AITL.[13] EBER$^+$ cells were localized in germinal centers in 1 type IV case (case LN25); this case also displayed epithelioid granuloma (Fig. 2). All 9 patients with EBER$^+$ type IV IgG4-related lymphadenopathy had systemic lymphadenopathy and/or extranodal involvement. PCR studies for TCR and IGH rearrangements did not demonstrate evidence of clonal T or B cells in 5/5 tested cases (LNs 2, 11, 12, 13, and 14).

Comparison Between EBER$^+$ and EBER$^-$ Cases

There were no differences in age between EBER$^+$ (51 to 76 y; mean ± SD, 64.0 ± 10.2 y) and EBER$^-$ cases (36

TABLE 3. Summary of Clinicopathologic Features of IgG4-related Lymphadenopathy

	Type I (n = 3)	Type II (n = 4)	Type III (n = 8)	Type IV (n = 16)
Age (y)				
Mean ± SD	63.6 ± 8.9	61.5 ± 19	72.5 ± 6.9	61.5 ± 10.8
> 50 y old (n [%])	3 (100)	3 (75)	8 (100)	13 (81)
> 60 y old (n [%])	1 (33)	3 (75)	7 (88)	11 (69)
Sex (Male/Female)	3/0	1/3	6/2	14/2
The number of IgG4$^+$ cells (/HPF)				
Mean ± SD	345 ± 116	155 ± 13.3	337 ± 47.3	198 ± 81.6
IgG4$^+$/IgG$^+$ plasma cell ratio (%)				
Mean ± SD	84.0 ± 14.3	50.2 ± 10.5	73.2 ± 12.7	72.5 ± 15.4
Disease distribution (n [%])				
Localized lymphadenopathy	0 (0)	0 (0)	0 (0)	4 (25)
Systemic lymphadenopathy	3 (100)	4 (100)	8 (100)	2 (13)
With extranodal involvement	1 (33)	3 (75)	3 (38)	12 (75)
EBER-ISH positivity	2 (75)	2 (50)	5 (63)	9 (56)
Distribution (n [%])				
Interfollicular/scattered	2 (100)	2 (100)	3 (60)	8 (88)
Intrafollicular/localized	0 (0)	0 (0)	0 (0)	1 (12)
Diffuse	0 (0)	0 (0)	2 (40)	0 (0)
Age (n [%])				
> 50 y old	2 (100)	1 (50)	5 (100)	8 (88)
> 60 y old	1 (50)	1 (50)	4 (80)	7 (77)

© 2014 Lippincott Williams & Wilkins

Copyright © Lippincott Williams & Wilkins. Unauthorized reproduction of this article is prohibited.

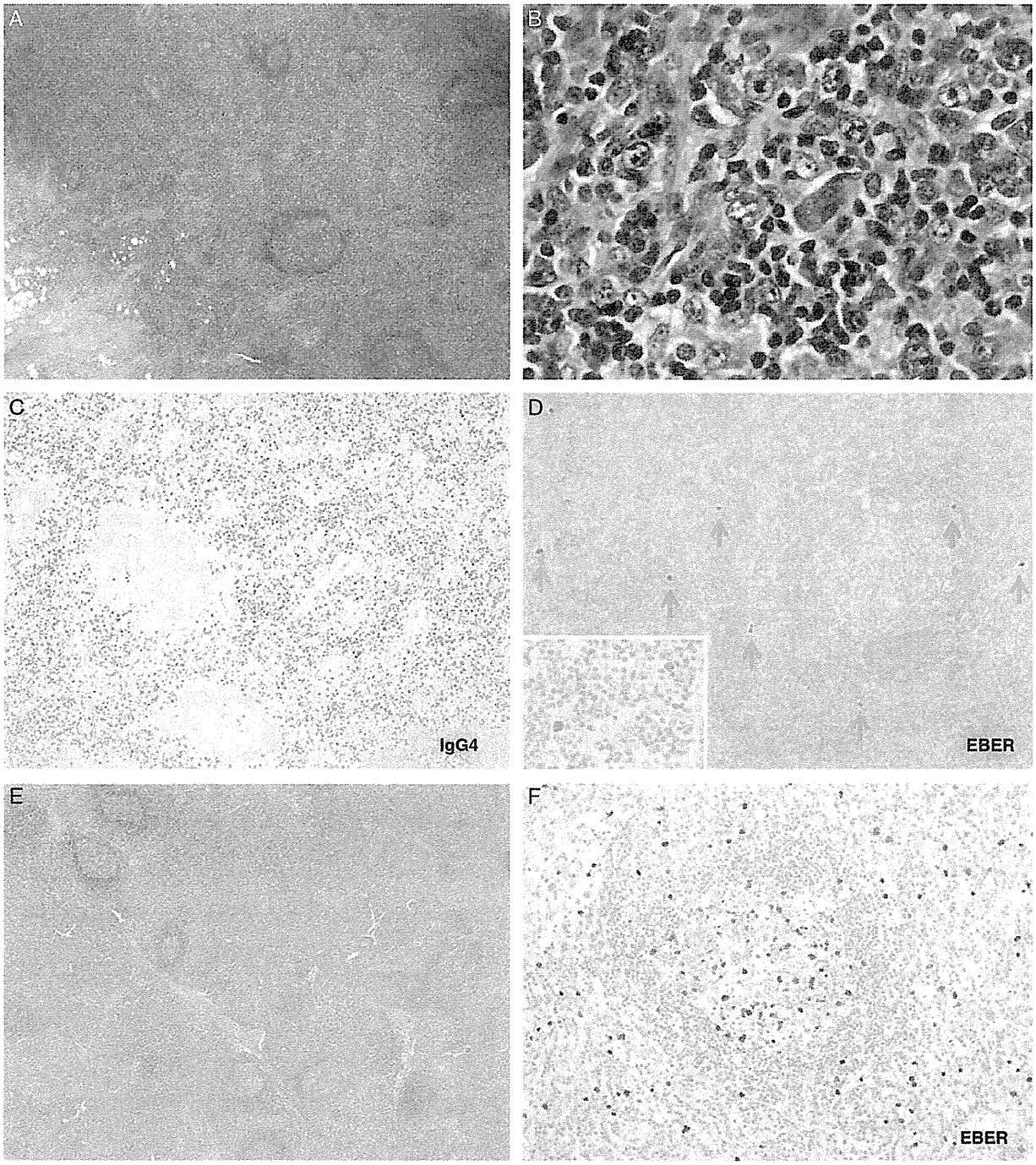

FIGURE 1. Histologic and immunohistochemical studies on type III IgG4-related lymphadenopathy (A–D, LN14; E–F, LN13). A and B, Expanded interfollicular area reveals polymorphous population consisting of mature and immature plasma cells, eosinophils, and numerous immunoblasts with small vessel proliferation (A and B, H&E). C, IgG4$^+$ plasma cells (C, IgG4). D, Small to large EBER-ISH$^+$ cells (133/0.5 cm^2) in the interfollicular area (D, EBER-ISH). E, Expanded interfollicular areas of LN13 (E, H&E). F, Diffuse infiltration of EBER$^+$ cells (F, EBER-ISH). H&E indicates hematoxylin and eosin.

to 82 y; mean ± SD, 65.3 ± 13.8 y) of IgG4-related lymphadenopathy ($P = 0.764$). There was also no difference in serum IgG levels between EBER$^+$ (mean ± SD, 3115 ± 1468 mg/dL; n = 15) and EBER$^-$ (mean ± SD, 2748 ± 1581 mg/dL; n = 12) cases ($P = 0.539$). There was no significant difference in the numbers of FOXP3$^+$ cells

© 2014 Lippincott Williams & Wilkins

Copyright © Lippincott Williams & Wilkins. Unauthorized reproduction of this article is prohibited.

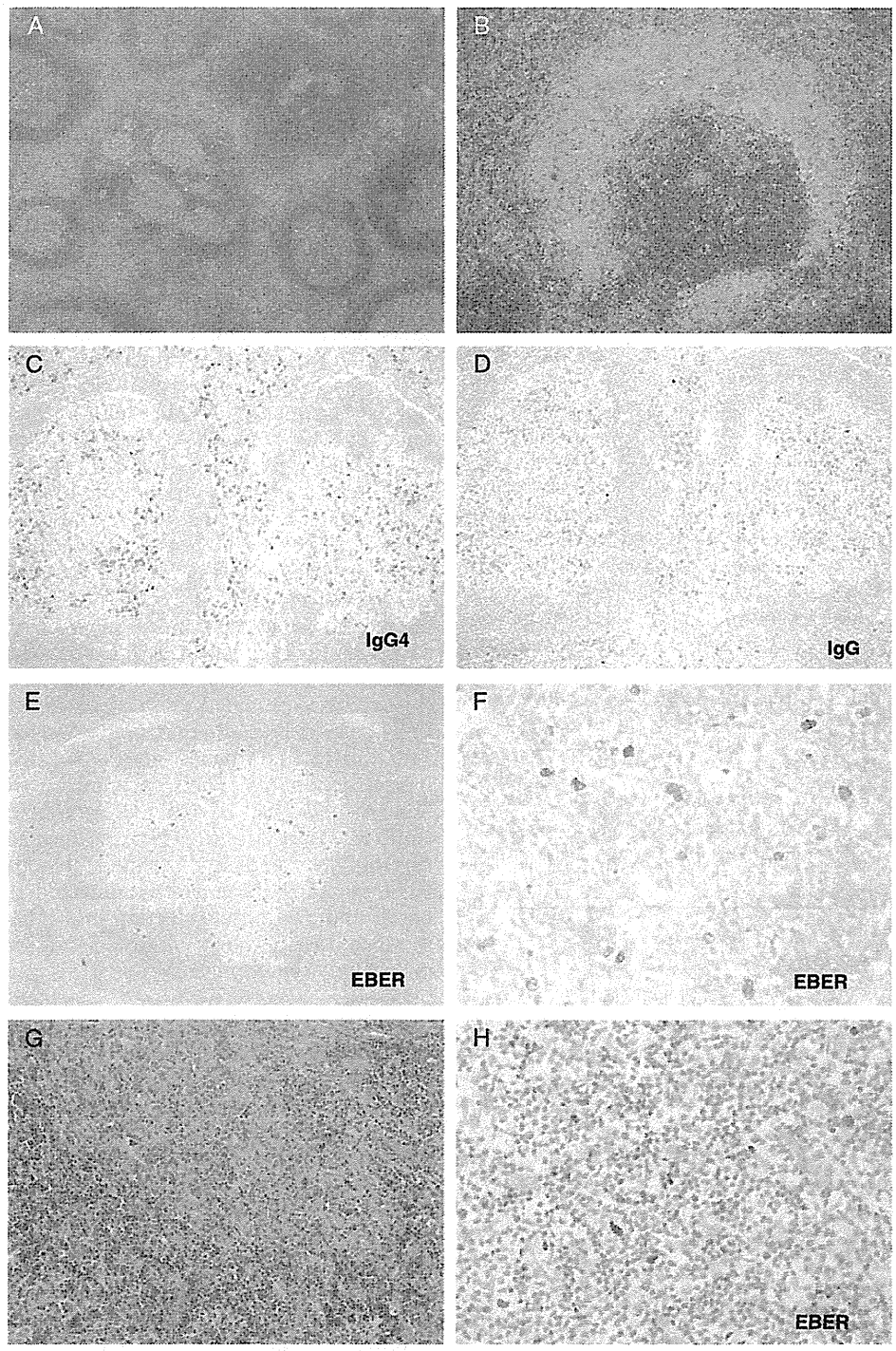

FIGURE 2. Histologic and immunohistochemical features of PTGC-type IgG4-related lymphadenopathy (LN25). A, PTGC-like germinal centers are observed (H&E). B, Epithelioid granuloma (H&E). C and D, Numerous $IgG4^+$ cells are localized in germinal centers. $IgG4^+/IgG^+$ cell ratio is >40% (C, IgG4; D, IgG). E and F, Many EBER-ISH^+ cells localize in a PTGC-like germinal center (E and F, EBER-ISH). G and H, IgG4-related lacrimal gland disease in the same patient (Ex7). G, Fibrosis and lymphoplasmacytic infiltration (H&E). H, Increased $EBER^+$ lymphocytes (56/0.5 cm^2) (EBER-ISH). H&E indicates hematoxylin and eosin.

© 2014 Lippincott Williams & Wilkins

Copyright © Lippincott Williams & Wilkins. Unauthorized reproduction of this article is prohibited.

between EBER$^+$ (mean ± SD, 304 ± 134; n = 11) and EBER$^-$ (mean ± SD, 322 ± 189; n = 8) cases ($P = 0.809$).

IgG4$^-$ Reactive Lymphoid Hyperplasia

Clinicopathologic and demographic characteristics of IgG4$^-$ reactive lymphoid hyperplasia are listed in Table 4. The age distribution was similar to that of the patients with IgG4-related lymphadenopathy and ranged from 50 to 85 years (mean ± SD, 67.1 ± 12.0). There were 18% of cases (4/22) with > 10 EBER$^+$ cells/0.5 cm^2 (ranging from 35 to 395/0.5 cm^2; mean ± SD, 155 ± 162), a significantly lower proportion than was seen in cases of IgG4-related lymphadenopathy ($P = 0.002$).

Extranodal IgG4-related Disease

The clinicopathologic findings for cases of extranodal IgG4-related diseases are listed in Tables 5 and 6. Greater than 10 EBER$^+$ cells/0.5 cm^2 were detected in 3 of 9 cases (33%) of IgG4-related lacrimal gland disease, 2 of 10 cases (20%) of IgG4-related submandibular gland disease, 0 of 2 cases (0%) of IgG4-related skin disease, and 0 of 3 cases of IgG4-related pancreatitis (Fig. 3). Although cases Ex4 and Ex7 had EBER$^+$ lymph nodes, only case Ex7 had EBV positivity in the lacrimal gland (Fig. 2G, H). In total, > 10 EBER$^+$ cells/0.5 cm^2 were detected in 5 of 24 (21%) extranodal IgG4-related biopsies, which was significantly less frequent than IgG4-related lymphadenopathy ($P = 0.006$).

IgG4$^+$ Cells in AITL

Seven cases showed few IgG4$^+$ cells (0 to 5/HPF). Three cases revealed scattered IgG4$^+$ cells (19, 24, and 47/HPF, respectively); none was in the range of the cases with nodal IgG4-related disease. In addition, overall, there were significantly fewer IgG4$^+$ cells present compared with type III IgG4-related lymphadenopathy (mean ± SD, 10.6 ± 15.3 compared with 337 ± 47.3) ($P < 0.001$).

TABLE 4. Clinicopathologic Features of IgG4$^-$ Reactive Lymphoid Hyperplasia

No.	Age/Sex	Affected Lymph Nodes	EBER-ISH$^+$ Cells (/0.5 cm^2)
RLH1	84/F	Cervix	103
RLH2	69/M	Para-aorta	0
RLH3	79/M	Axilla	0
RLH4	78/F	Inguen	6
RLH5	79/F	Mediastinum	0
RLH6	69/F	Inguen	0
RLH7	63/F	Cervix	0
RLH8	51/F	Inguen	5
RLH9	56/F	Cervix	0
RLH10	50/M	Cervix	395
RLH11	52/M	Cervix	8
RLH12	80/M	Inguen	2
RLH13	78/M	Cervix	1
RLH14	85/F	Axilla	4
RLH15	59/M	Inguen	7
RLH16	72/M	Cervix	0
RLH17	62/M	Inguen	35
RLH18	55/F	Abdomen	0
RLH19	55/F	Axilla	0
RLH20	67/F	Axilla	90
RLH21	53/F	Axilla	4
RLH22	82/M	Cervix	0

F indicates female; M, male; RLH, reactive lymphoid hyperplasia.

DISCUSSION

Very limited previous reports have indicated a possible relationship between IgG4-related disease and EBV. Acute EBV mononucleosis has been reported to be associated with a transient 75% increase in mean serum IgG4 levels.[14] A case of EBV-related lymphadenopathy has been reported that mimicked the clinical features of IgG4-related disease, with an elevated serum IgG4 level but without many IgG4$^+$ cells in the biopsied lymph nodes.[15] EBV$^+$ classical Hodgkin lymphoma was found in a patient with IgG4-related cervical fibrosis.[16] An EBV$^+$ inflammatory pseudotumor-like follicular dendritic cell sarcoma was also reported to have numerous IgG4$^+$ cells.[17] The authors discussed a relationship between EBV-related immune dysfunction and the proliferation of IgG4$^+$ cells. Although these reports mentioned some relationship between EBV and increase of IgG4, EBV infection in IgG4-related disease has not been examined except for a single case report.[5] Hence, this study investigated the relationship between EBV and IgG4-related disease. Increased EBV-infected cells were found in 18 of 31 lymph nodes (58%) with IgG4-related lymphadenopathy. This proportion was significantly higher than that of reactive lymphoid hyperplasia in similarly aged group, which confirmed the clear relationship between IgG4-related lymphadenopathy and EBV. As most Japanese are infected by EBV in childhood, and new onset infection in adulthood is very rare, the increased numbers of EBV$^+$ cells was considered to most likely represent EBV reactivation rather than acute infection.

Type III IgG4-related lymphadenopathy has distinct histologic features, including interfollicular lymphoplasmacytic infiltration, angiogenesis, and many immunoblasts, which mimic AITL.[1] In this study, only a few scattered IgG4$^+$ cells were detected in AITL, which indicated that IgG4$^+$ cell proliferation was not simply induced by EBV reactivation or dysfunction of helper T cells. There is a possibility that both IgG4-related disease and EBV reactivation are induced by other factors.

Type IV cases are usually localized in submandibular lymph nodes, although approximately 50% of cases have extranodal involvement. Less than 10% develop systemic lymphadenopathy.[2] In contrast, in this study, all the patients with type IV IgG4-related lymphadenopathy with EBV reactivation developed systemic lymphadenopathy and/or extranodal involvement. The lymph node in 1 EBV$^+$ type IV case had epithelioid granulomas, which was similar to a previously reported case of EBV$^+$ IgG4-related lymphadenopathy.[5] Cases of IgG4-related lymphadenopathy with epithelioid granulomas have been reported sporadically.[18] Of interest,

© 2014 Lippincott Williams & Wilkins

Copyright © Lippincott Williams & Wilkins. Unauthorized reproduction of this article is prohibited.

TABLE 5. Clinicopathologic Features of Extranodal IgG4-related Diseases

No.	Age/Sex	Affected Organs	Average IgG4$^+$ Cells (/HPF)	EBER-ISH$^+$ Cells (/0.5 cm^2)	Other Lesions
Ex1	56/F	Lacrimal gland	111	1	
Ex2	60/F	Lacrimal gland	282	1	
Ex3	49/M	Lacrimal gland	377	9	
Ex4*	36/F	Lacrimal gland	239	2	Cervical lymph node
Ex5	61/M	Lacrimal gland	373	0	
Ex6	39/F	Lacrimal gland	301	0	
Ex7†	68/M	Lacrimal gland	204	56	Submandibular lymph node
Ex8	67/F	Lacrimal gland	177	175	
Ex9	72/M	Lacrimal gland	231	542	
Ex10	57/F	Submandibular gland	109	0	
Ex11	57/F	Submandibular gland	144	0	Parotid gland
Ex12	59/M	Submandibular gland	190	1	
Ex13	61/M	Submandibular gland	216	5	
Ex14	69/M	Submandibular gland	435	7	
Ex15	76/M	Submandibular gland	160	3	
Ex16	66/F	Submandibular gland	404	2	
Ex17	59/F	Submandibular gland	264	0	
Ex18	69/M	Submandibular gland	307	66	
Ex19	67/M	Submandibular gland	224	157	
Ex20	65/M	Skin	189	0	
Ex21	63/F	Skin	46	0	Parotid gland
Ex22	69/M	Pancreas	195	0	
Ex23	61/M	Pancreas	437	0	
Ex24	64/M	Pancreas	76	0	

*The same patient had IgG4-related lymphadenopathy listed in Table 1 (LN6).
†The same patient had IgG4-related lymphadenopathy listed in Table 1 (LN25).
Ex indicates extranodal; F, female; M, male.

EBER$^+$ cells were localized in germinal centers in this type IV case with epithelioid granuloma. There are reports of EBV$^+$ nonendemic Burkitt lymphoma associated with epithelioid granulomas.[19,20] The significance of this finding is still unclear.

EBV-infected cells are usually observed and studied in the lymph nodes, where the virus is known to remain in the dormant stage for many years.[10] In this study, increased numbers of EBER$^+$ cells were significantly more frequently observed in IgG4-related lymphadenopathy than in extranodal IgG4-related disease. The proportion of EBV$^+$ cases was similar between extranodal IgG4-related disease and non–IgG4-related reactive lymphoid hyperplasia ($P = 0.559$). Increased numbers of EBV-infected cells may be observed more frequently in lymph nodes than in other sites. Lacrimal glands and salivary glands seemed to have increased numbers of EBV-infected cells more frequently than other extranodal sites; however, the number of extranodal samples was too small for a meaningful statistical analysis.

Although our study clearly suggested a relationship between IgG4-related disease and EBV, the precise mechanism remains unclear. Whether IgG4-related disease directly or indirectly induces expansion of EBV-infected cells, possibly related to EBV reactivation, or is secondary to EBV infection is unknown. As mentioned above, acute EBV infection can lead to an increase in the serum IgG4 level. However, in other situations like AITL, EBV-infected cells do not lead to increased numbers of IgG4$^+$ cells, suggesting that IgG4 lymphadenopathy is not the direct effect of EBV infection and that the increased number of EBV$^+$ cells, present in only a subset of cases, is somehow related to the IgG4 disease.

Because of concern as to whether the expansion of EBV-infected cells in many cases of IgG4-related lymphadenopathy could simply reflect an age-related phenomenon, a group of non–IgG4-related reactive lymph nodes were studied for comparison purposes. This patient cohort did not show a difference in age from the patients with IgG4-related disease but had significantly fewer cases with increased EBV-infected cells. In addition, there was no significant difference in age distribution between EBER$^+$ and EBER$^-$ IgG4-related disease cases. Therefore, age does not seem to be a factor in the association of IgG4-related nodal disease with increased numbers of EBV-infected cells.

Upregulation of Treg and helper T-cell (Th2) activity has been reported in tissues with IgG4-related

TABLE 6. Summary of Clinicopathologic Features of IgG4-related Diseases

	Lymph Node (n = 31)	Lacrimal Gland (n = 9)	Submandibular Gland (n = 10)	Skin (n = 2)	Pancreas (n = 3)
Age (y)	64.5 ± 11.6	56.4 ± 12.7	64.0 ± 6.0	64.0 ± 1.4	64.6 ± 4.0
Sex	M:F = 24:7	M:F = 4:5	M:F = 6:4	M:F = 1:1	M:F = 3:0
EBER$^+$ cases (n [%])	18 (58)	3 (33)	2 (20)	0 (0)	0 (0)

© 2014 Lippincott Williams & Wilkins

Copyright © Lippincott Williams & Wilkins. Unauthorized reproduction of this article is prohibited.

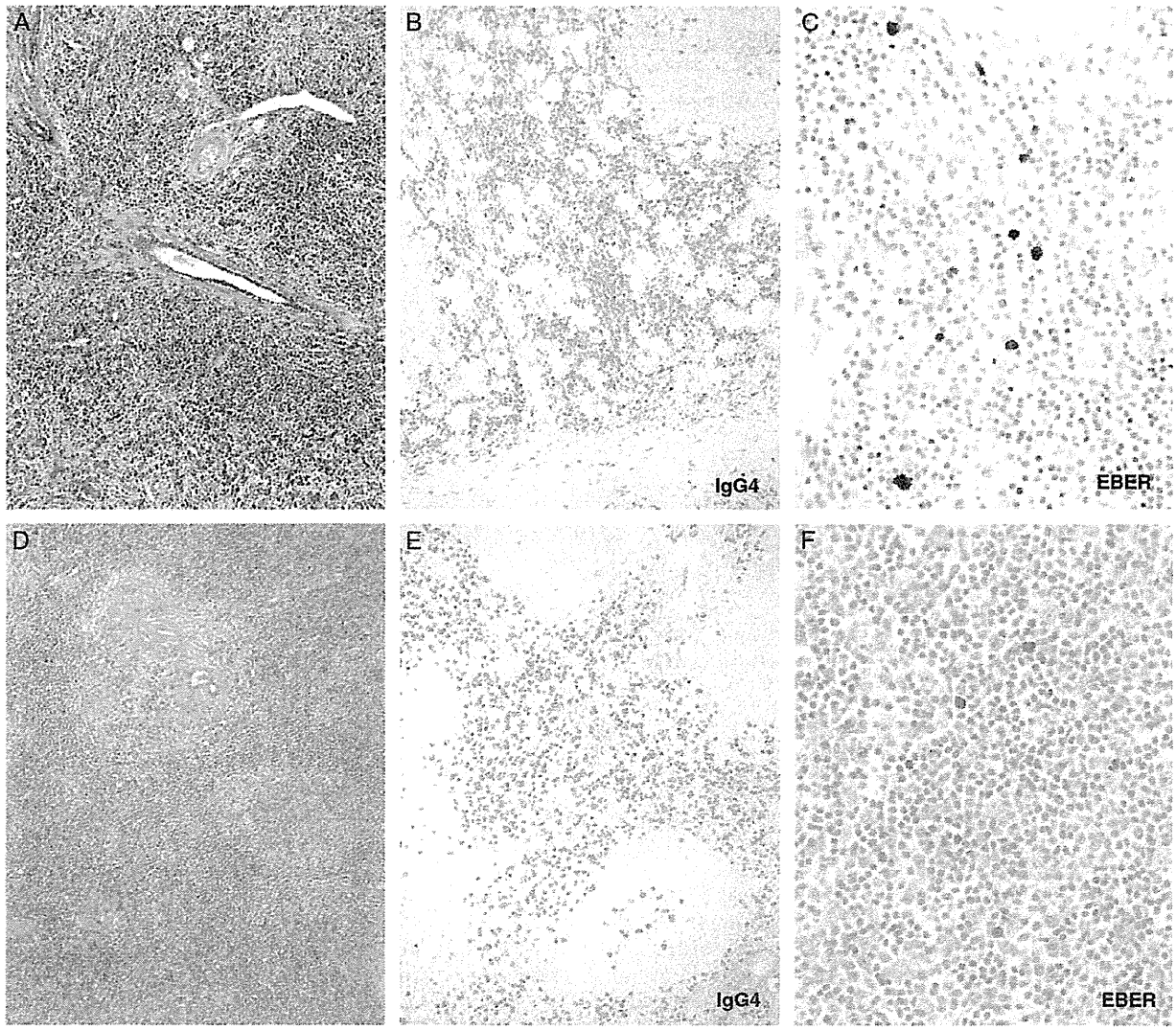

FIGURE 3. Analysis of extranodal IgG4-related disease: IgG4-related submandibular gland disease (Ex19). A, Lymphoplasmacytic infiltration and dense fibrosis. Salivary gland ducts remain intact (H&E). B, Numerous IgG4$^+$ cells (IgG4). C, Increased EBER$^+$ cells (157/0.5 cm^2) (EBER-ISH). D–F, IgG4-related lacrimal gland disease (Ex9). D, Infiltration of small lymphocytes and plasma cells (H&E). E, Significant IgG4$^+$ cells (IgG4). F, Increased EBER$^+$ cells (542/0.5 cm^2) (EBER-ISH). H&E indicates hematoxylin and eosin.

disease.[3] Although the precise mechanism of immune suppression by Treg is not fully understood, secretion of interleukin-10 and transforming growth factor β1 seems to be involved.[21] Although the relationship between Treg and EBV has not been fully investigated, upregulation of Treg activity might contribute to a disruption of immune balance. However, in our study, the number of FOXP3$^+$ Tregs was similar between EBER$^+$ and EBER$^-$ groups. Further study is required to understand the relationship between IgG4-related disease and EBV.

In conclusion, increased numbers of EBV-infected cells are frequently found in IgG4-related lymphadenopathy, including in the type III cases with many immunoblasts that can morphologically mimic AITL, and is not related to patient age. Distinction from AITL, however, was not difficult, in part because AITL never had sufficient IgG4 positivity to fulfill the criteria for IgG4-related lymphadenopathy. IgG4-related disease with increased numbers of EBER$^+$ cells may have some clinical implications as, in contrast to usual expectation, all the patients with EBV$^+$ type IV IgG4-related lymphadenopathy developed systemic lymphadenopathy and/or extranodal involvement. Finally, particularly given that IgG4-related lymphadenopathy often occurs in individuals over 50 years of age, it is important to recognize that it must be included in the differential diagnosis of EBV$^+$ lymphoproliferative disorders, including EBV$^+$ diffuse large B-cell lymphoma of the elderly.

© 2014 Lippincott Williams & Wilkins

Copyright © Lippincott Williams & Wilkins. Unauthorized reproduction of this article is prohibited.

ACKNOWLEDGMENTS

This work was supported by a Grant-in-Aid for Scientific Research (C) (no. 24591447) from the Japan Society for the Promotion of Science and 'Research on Measures for Intractable Disease' Project: matching fund subsidy from Ministry of Health Labour and Welfare, Japan.

REFERENCES

1. Sato Y, Notohara K, Kojima M, et al. IgG4-related disease: histological overview and pathology of hematological disorders. *Pathol Int*. 2010;60:247–258.
2. Sato Y, Inoue D, Asano N, et al. Association between IgG4-related disease and progressively transformed germinal centers of lymph nodes. *Mod Pathol*. 2012;35:956–967.
3. Zen Y, Fujii T, Harada K, et al. Th2 and regulatory immune reactions are increased in immunoglobin G4-related sclerosing pancreatitis and cholangitis. *Hepatology*. 2007;45:1538–1546.
4. Niedobitek G, Herbst H, Young LS, et al. Patterns of Epstein-Barr virus infection in non-neoplastic lymphoid tissue. *Blood*. 1992; 79:2520–2526.
5. Takahashi E, Kojima M, Kobayashi M, et al. Primary IgG4-related lymphadenopathy with prominent granulomatous inflammation and reactivation of Epstein-Barr virus. *Virchows Arch*. 2012;460: 225–229.
6. Deshpande V, Zen Y, Chan JK, et al. Consensus statement on the pathology of IgG4-related disease. *Mod Pathol*. 2012;25: 1181–1192.
7. Sato Y, Kojima M, Takata K, et al. Systemic IgG4-related lymphadenopathy: a clinical and pathologic comparison to multicentric Castleman's disease. *Mod Pathol*. 2009;22:589–599.
8. Sato Y, Takeuchi M, Takata K, et al. Clinicopathologic analysis of IgG4-related skin disease. *Mod Pathol*. 2013;26:523–532.
9. Dogan A, Gaulard P, Jaffe ES, et al. Angioimmunoblastic T-cell lymphoma. In: Swerdlow SH, Campo E, Harris NL, eds. *WHO Classification of Tumours of Haematopoietic and Lymphoid Tissues*. Lyon, France: International Agency for Research on Cancer; 2008: 309–311.
10. Dojcinov SD, Venkataraman G, Pittaluga S, et al. Age-related EBV-associated lymphoproliferative disorders in the Western population: a spectrum of lymphoid hyperplasia and lymphoma. *Blood*. 2011;117:4726–4735.
11. van Dongen JJ, Langerak AW, Bruggemann M, et al. Design and standardization of PCR primers and protocols for detection of clonal immunoglobulin and T-cell receptor gene recombinations in suspect lymphoproliferations: report of the BIOMED-2 Concerted Action BMH4-CT98-3936. *Leukemia*. 2003;17:2257–2317.
12. Miyata-Takata T, Takata K, Yamanouchi S, et al. Detection of T-cell receptor γ gene rearrangement in paraffin-embedded T or natural killer/T-cell lymphoma samples using the BIOMED-2 protocol. *Leuk Lymphoma*. 2014. [Epub ahead of print].
13. Federico M, Rudiger T, Bellei M, et al. Clinicopathologic characteristics of angioimmunoblastic T-cell lymphoma: analysis of the international peripheral T-cell lymphoma project. *J Clin Oncol*. 2013;31:240–246.
14. Shacks SJ, Heiner DC, Bahba SL, et al. Increased serum IgG4 levels in acute Epstein-Barr viral mononucleosis. *Ann Allergy*. 1985;54:284–288.
15. Wada Y, Kojima M, Yoshita K, et al. A case of Epstein-Barr virus-related lymphadenopathy mimicking the clinical features of IgG4-related disease. *Mod Rheumatol*. 2013;23:597–603.
16. Cheuk W, Tam F, Chan A, et al. Idiopathic cervical fibrosis-A new member of IgG4-related sclerosing diseases: report of 4 cases, 1 complicated by composit lymphoma. *Am J Surg Pathol*. 2010; 34:1678–1685.
17. Choe JY, Go H, Jeon YK, et al. Inflammatory pseudotumor-like follicular dendritic cell sarcoma of the spleen: a report pf six cases with increased IgG4+ cells. *Pathol Int*. 2013;63:245–251.
18. Zen Y, Nakamura Y. IgG4-related disease: a cross-sectional study of 114 cases. *Am J Surg Pathol*. 2010;34:1812–1819.
19. Haralambieva E, Rosati S, Noesel CN, et al. Florid granulomatous reaction in Epstein-Barr virus-positive nonendemic Burkitt lymphomas. *Am J Surg Pathol*. 2004;28:379–383.
20. Schrager JA, Pittaluga S, Raffeld M, et al. Granulomatous reaction in Burkitt lymphoma: correlation with EBV positivity and clinical outcome. *Am J Surg Pathol*. 2005;29:1115–1116.
21. Wingate PJ, McAulay KA, Anthony IC, et al. Regulatory T cell activity in primary and persistent Epstein-Barr virus infection. *J Med Virol*. 2009;81:870–877.

© 2014 Lippincott Williams & Wilkins

Copyright © Lippincott Williams & Wilkins. Unauthorized reproduction of this article is prohibited.

J Infect Chemother (2013) 19:750–753
DOI 10.1007/s10156-012-0488-2

CASE REPORT

Coadministration of tenofovir decreased atazanavir plasma concentration after unilateral nephrectomy

Yusuke Kunimoto · Hiroshi Yasui · Norifumi Touda · Masako Okazaki · Hiromasa Nakata · Norimasa Noda · Hiroshi Ikeda · Toshiaki Hayashi · Satoshi Takahashi · Yasuhisa Shinomura · Tadao Ishida · Atsushi Miyamoto

Received: 1 August 2012 / Accepted: 18 September 2012 / Published online: 5 October 2012
© Japanese Society of Chemotherapy and The Japanese Association for Infectious Diseases 2012

Abstract We report a case in which the atazanavir (ATV) concentration in the plasma decreased after unilateral nephrectomy in a patient receiving tenofovir (TDF). The patient was a 39-year-old man diagnosed with human immunodeficiency virus type 1 infection and was being treated with TDF/emtricitabine, ATV, and ritonavir. Before nephrectomy, ATV and TDF plasma trough concentrations were 810 and 65 ng/ml, respectively. At this time, estimated glomerular filtration rate (eGFR) was 111 ml/min/1.73 m^2. Approximately 5 months after starting antiretroviral therapy (ART), the patient underwent nephrectomy. Plasma concentrations were remeasured 18 weeks after the operation, and the TDF concentration had increased to 109 ng/ml, whereas the ATV concentration decreased to 290 ng/ml. His eGFR decreased to 50 ml/min/1.73 m^2 at the time of the second measurement. The decreased ATV plasma concentration suggested that interactions between ATV and TDF were exacerbated by an increase in TDF plasma concentration caused by renal dysfunction. This case report suggests that it is important to monitor the ATV plasma concentration to ensure that it is no less than the target trough concentration when renal function decline is observed in patients receiving ART including ATV and TDF.

Keywords Atazanavir · Tenofovir · Human immunodeficiency virus type 1 · Therapeutic drug monitoring · Drug interaction · Nephrectomy

Y. Kunimoto (✉) · N. Touda · M. Okazaki · H. Nakata · N. Noda · A. Miyamoto
Department of Hospital Pharmacy, Sapporo Medical University Hospital, South 1, West 16, Chuo-ku, Sapporo, Hokkaido 060-8543, Japan
e-mail: kunimoto@sapmed.ac.jp

H. Yasui · H. Ikeda · T. Hayashi · Y. Shinomura · T. Ishida
First Department of Internal Medicine, Sapporo Medical University School of Medicine, Sapporo, Japan

H. Yasui
Department of Regional Health Care and Medicine, Sapporo Medical University School of Medicine, Sapporo, Japan

S. Takahashi
Department of Urology, Sapporo Medical University School of Medicine, Sapporo, Japan

Introduction

Antiretroviral therapy (ART) has resulted in significant improvement in the survival of human immunodeficiency virus type 1 (HIV-1)-infected patients since the introduction of HIV-1 protease inhibitors (PIs) [1, 2]. ART usually consists of two nucleoside reverse transcriptase inhibitors (NRTIs), with a ritonavir (RTV)-boosted PI, non-NRTI, or integrase inhibitor [3]. Atazanavir (ATV) is a member of the PI class of antiretroviral (ARV) drugs, recommended as one of the preferred agents by the guidelines for the initiation of treatment when coadministered with the strong CYP3A4 inhibitor RTV [3]. Tenofovir (TDF) is grouped with the NRTI class of ARV drugs and is a preferred component of the first-line regimen in the guidelines.

Therapeutic drug monitoring (TDM), an important clinical technique in personalized medicine, is currently widely applied in medical treatments using antibiotics, immunosuppressive agents, antiepileptic agents, and other drugs [4–6]. In ART, TDM is recommended in specific clinical scenarios such as cases in which pathophysiological changes (e.g., renal dysfunction) or drug–drug interactions adversely affect pharmacokinetics [3]. However, TDM for ART is not recommended for routine use in the

clinical care of HIV-1-infected patients because of a lack of large prospective studies showing that TDM improves clinical or virological outcomes [3]. TDM is still not a generally accepted strategy in ART at clinical sites. By contrast, data from small studies showed that TDM for ART improves virological response and decreases the incidence of concentration-related drug toxicity [7, 8]. Nevertheless, although TDM may provide clinical utility to HIV-1-infected patients, further clinical evidence is needed to assess the usefulness of TDM in ART.

We report a case of changes in ATV plasma concentration before and after unilateral nephrectomy. Our report suggests that it is important to consider changes in ARV drug plasma concentrations caused by to drug–drug interactions and decline in renal function. Informed consent was obtained from the patient for publication of this report.

Case report

A 39-year-old Japanese man was admitted to our hospital with fever, coughing, and dyspnea. He was diagnosed with HIV-1 infection and pneumocystis pneumonia after admission. On day 2 after admission, blood laboratory results showed the following: $CD4^+$ T-cell count, 51 cells/μl, and HIV RNA, 2.5×10^5 copies/ml. He was initially treated with sulfamethoxazole-trimethoprim for 21 days. After completion of the treatment, we started ART with TDF/emtricitabine (FTC), ATV, and RTV.

On day 3 after starting ART, we performed a computed tomography scan for follow-up on pneumonia, and incidentally found a renal mass suggestive of renal cell carcinoma (RCC). The patient was diagnosed with suspected RCC (cT1aN0M0). On day 37 after starting ART, we measured plasma concentrations of ATV and TDF, as follows. Pre-dose blood samples were collected in heparinized tubes and centrifuged for 10 min at $3{,}000 \times g$; the resultant plasma was removed and stored at −20 °C until analysis. ATV plasma concentration was analyzed using liquid chromatography–tandem mass spectrometry, and TDF plasma concentration was analyzed by high-performance liquid chromatography. ATV and TDF plasma concentrations were 810 and 65 ng/ml, respectively. The ATV plasma concentration was higher than that of the target trough (150 ng/ml) specified in the American Department of Health and Human Services (DHHS) guidelines [3].

On day 149 after starting ART, the patient underwent radical nephrectomy of the right kidney; adjuvant chemotherapy was not performed. His serum creatinine was higher post-nephrectomy than pre-nephrectomy. We were concerned about further deterioration of renal function and, therefore, switched from TDF/FTC to abacavir/lamivudine (3TC). However, the patient's ART was changed again to TDF/FTC because of the appearance of persistent skin rash and itching sensation. We selected TDF/FTC because it has excellent efficacy, a favorable toxicity profile, and a convenient dosage schedule in comparison with those of zidovudine/3TC. On day 277 after starting ART, we anticipated that renal dysfunction after nephrectomy might affect the pharmacokinetics of ATV and TDF, and remeasured these plasma concentrations. We found that the TDF plasma concentration increased to 109 ng/ml; although the ATV plasma concentration was maintained at the target trough concentration, it decreased to 290 ng/ml. His viral load was undetectable (less than 40 copies/ml) on day 327 after starting ART.

At the time of both measurements of ARV drug plasma concentrations, the patient took ATV with food. In addition, the patient did not use medications that interact with ARV drugs. There was no significant difference in the time to blood sampling for TDM from the time that the patient took the ARV drugs. There were no appreciable signs of altered liver function, such as changes in plasma concentration of ATV (Table 1). Figure 1 outlines the clinical course of the patient.

Discussion

In this report, we focused on changes in plasma concentration of ARV drugs induced by decreased renal function after unilateral nephrectomy. TDF plasma concentration was increased, whereas ATV plasma concentration was decreased in our patient after the operation. Because low ATV concentration may lead to virological failure [10, 11], we believe that detailed analysis of the patient's course may help to prevent treatment failure with ART that includes ATV and TDF.

TDF is a renally eliminated drug excreted by glomerular filtration and active tubular secretion. Previous reports have documented increases in TDF concentration caused by decline in renal function [12]. Julien et al. [13] reported that serum creatinine level and creatinine clearance rate affected TDF clearance. Our patient also showed increased TDF plasma concentration after decline in renal function following nephrectomy, consistent with previous findings. ATV is eliminated primarily by the liver. The renal elimination of unchanged ATV was approximately 7 % of the administered dose [14]. The ATV minimum concentration was reportedly 96 % higher in subjects with severe renal impairment than in those with normal renal function [14]. In contrast, although the ATV plasma concentration in our case was above the target trough concentration before nephrectomy, its post-nephrectomy concentration fell to near the target trough concentration despite reduced renal function.

Table 1 Liver function tests at the time of therapeutic drug monitoring (TDM)

Laboratory tests	At the first time of TDM	At the second time of TDM
AST (IU/l)	21	17
ALT (IU/l)	20	21
ALP (IU/l)	225	273
TBIL (mg/dl)	1.2	2.0
DBIL (mg/dl)	0.3	0.5
IBIL (mg/dl)	0.9	1.5
ChE (IU/l)	248	281

AST aspartate aminotransferase, *ALT* alanine aminotransferase, *ALP* alkaline phosphatase, *TBIL* total bilirubin, *DBIL* direct bilirubin, *IBIL* indirect bilirubin, *ChE* cholinesterase

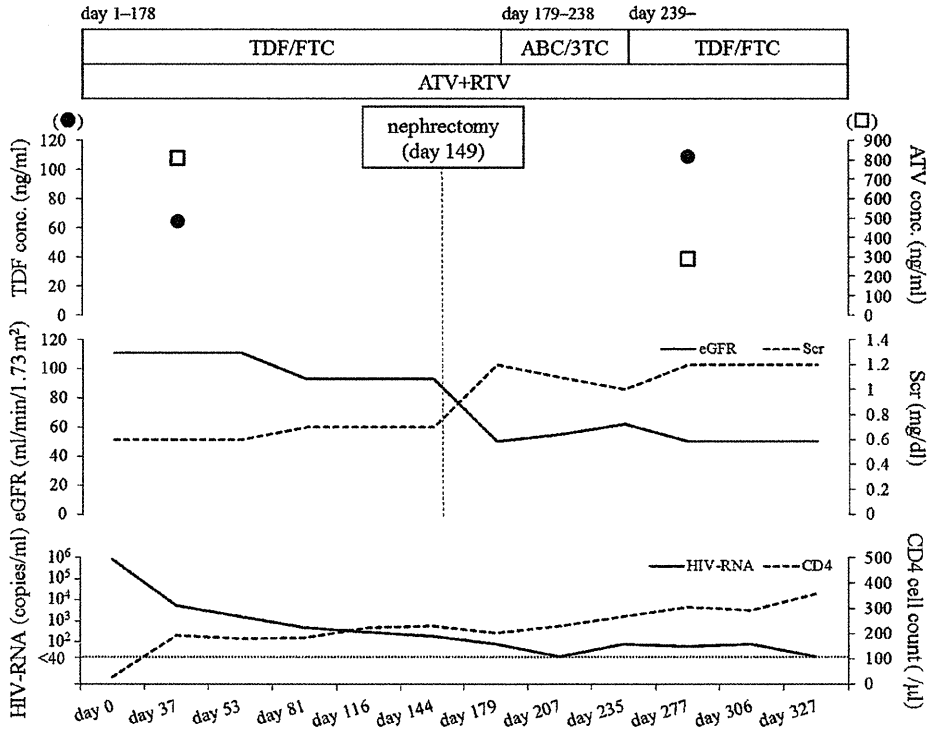

Fig. 1 Clinical course. *Upper panel*: *circles* and *squares* indicate concentrations of tenofovir (*TDF*) and atazanavir (*ATV*), respectively. *Middle panel*: *solid line* indicates estimated glomerular filtration rate (*eGFR*). The eGFR was calculated using the Modification of Diet in Renal Disease Study formula [9]. *Dashed line* shows serum creatinine levels (*Scr*). *Lower panel*: *solid* and *dashed lines* show HIV-RNA and $CD4^+$ T-cell count (CD4 cell count) in peripheral blood. *FTC* emtricitabine, *ABC* abacavir, *3TC* lamivudine, *RTV* ritonavir

To date, no study has reported a decline in ATV concentration following a decline in renal function. The pharmacokinetics of ATV are also affected by liver function, and doses of ATV must be reduced in patients with hepatic impairment [3]. However, in our case, there was no obvious difference in aspartate aminotransferase, alanine aminotransferase, alkaline phosphatase, direct bilirubin, and cholinesterase levels between the two ATV plasma concentration measurements (Table 1). We believe that elevation of indirect bilirubin was caused by inhibition of UDP-glucuronosyl transferase by ATV. We conclude that liver function had no effect on the change in ATV plasma concentration in our case.

This case report suggests that decreased ATV plasma concentration was strongly influenced by drug interactions between ATV and TDF. Although the mechanism of this interaction is still unclear, coadministration of ATV and TDF causes a decrease in ATV plasma concentration [10]. Taburet et al. [10] reported the possibility that TDF acts as a P-glycoprotein (P-gp) inducer and thereby decreases the concentration of ATV, which is a substrate of P-gp. In this case, the decreased ATV plasma concentration may be attributed to increased TDF plasma concentration brought about by the decline in renal function after nephrectomy. Increased TDF plasma concentration may further induce P-gp, in turn affecting ATV levels. The minimum concentration of ATV when coadministered with TDF can reportedly maintain the target trough concentration by combination with RTV, a potent CYP3A4 inhibitor [15]. However, our experience suggests that it is important to monitor the ATV plasma concentration to ensure that it is no less than the target trough when renal function decline is observed in patients receiving ART including ATV and TDF.

In routine clinical care of HIV-1-infected patients, ARV drug doses are not adjusted on the basis of plasma concentrations of drugs. Currently, when altered drug plasma concentrations are thought to be involved in virological failure or side effects, it is important to examine the patient's adherence and pharmacokinetic issues (e.g., food/fasting requirements for each ARV drug, or malabsorption from gastrointestinal symptoms such as vomiting or diarrhea) [3]. If there are no problems with adherence and pharmacokinetic issues, changes to other ARV drugs can be considered. However, patients who experience side effects of ART may exhibit resistance to changes in ARV drugs. In such cases, if the implementation of TDM leads to maintenance of antiviral effects and mitigation of side effects, treatment options will greatly expand.

We think that the variations in ARV drug plasma concentrations observed in our case were caused by the decline in renal function and drug interactions between ATV and TDF. Renal dysfunction is one of the most notable side effects of TDF, although our case is unique in that nephrectomy occurred after the start of ART. Nevertheless, previous reports have shown that ART including TDF is significantly associated with decline in renal function [16–19]. These findings suggest that patients can exhibit increased TDF plasma concentration because of a decline in renal function. For this reason, the possibility of decreased ATV plasma concentration, as shown by this article, may be important.

There are several unresolved issues in this case. First, we performed only two measurements of ARV drug plasma concentration. Therefore, we cannot consider intraindividual variation in ATV levels. Second, we did not adjust the dose of ATV because there is little evidence of efficacy and safety of modified-dose ATV in ART. In the future, we think that it is necessary to demonstrate the effectiveness of ATV dose adjustment based on TDM. In conclusion, our case highlights the possibility of decreased ATV plasma concentration induced by increased TDF plasma concentration caused by declining renal function.

Acknowledgments This work was supported by the Research Project on HIV/AIDS, Hokkaido Government.

Conflict of interest None.

References

1. The Antiretroviral Therapy Cohort Collaboration. Life expectancy of individuals on combination antiretroviral therapy in high-income countries: a collaborative analysis of 14 cohort studies. Lancet. 2008;372:293–9.
2. Cooper DA. Life and death in the cART era. Lancet. 2008;372:266–7.
3. Panel on Antiretroviral Guidelines for Adults and Adolescents. Guidelines for the use of antiretroviral agents in HIV-1-infected adults and adolescents. Department of Health and Human Services. http://www.aidsinfo.nih.gov/contentfiles/lvguidelines/adultandadolescentgl.pdf. Accessed 15th Aug 2012.
4. Rybak M, Lomaestro B, Rotschafer JC, Moellering R Jr, Craig W, Billeter M, et al. Therapeutic monitoring of vancomycin in adult patients: a consensus review of the American Society of Health-System Pharmacists, the Infectious Diseases Society of America, and the Society of Diseases Pharmacists. Am J Health Syst Pharm. 2009;66:82–98.
5. Monchaud C, Marquet P. Pharmacokinetic optimization of immunosuppressive therapy in therapy in thoracic transplantation: part I. Clin Pharmacokinet. 2009;48:419–62.
6. Johannessen SI, Landmark CJ. Value of therapeutic drug monitoring in epilepsy. Expert Rev Neurother. 2008;8:929–39.
7. Fletcher CV, Anderson PL, Kakuda TN, Schacker TW, Henry K, Gross CR, et al. Concentration-controlled compared with conventional antiretroviral therapy for HIV infection. AIDS. 2002;16:551–60.
8. Fabbiani M, Di Giambenedetto S, Bracciale L, Bacarelli A, Ragazzoni E, Cauda R, et al. Pharmacokinetic variability of antiretroviral drugs and correlation with virological outcome: 2 years of experience in routine clinical practice. J Antimicrob Chemother. 2009;64:109–17.
9. Levey AS, Bosch JP, Lewis JB, Greene T, Rogers N, Roth D. A more accurate method to estimate glomerular filtration rate from serum creatinine: a new prediction equation. Ann Intern Med. 1999;130:461–70.
10. Taburet AM, Piketty C, Chazallon C, Vincent I, Gerard L, Calvez V, et al. Interactions between atazanavir–ritonavir and tenofovir in heavily pretreated human immunodeficiency virus-infected patients. Antimicrob Agents Chemother. 2004;48:2091–6.
11. Fabbiani M, Di Giambenedetto S, Ragazzoni E, Colafigli M, Prosperi M, Cauda R, et al. Mid-dosing interval concentration of atazanavir and virological outcome in patients treated for HIV-1 infection. HIV Med. 2010;11:326–33.
12. Kearney BP, Yale K, Shah J, Zhong L, Flaherty JF. Pharmacokinetics and dosing recommendations of tenofovir disoproxil fumarate in hepatic or renal impairment. Clin Pharmacokinet. 2006;45:1115–24.
13. Julien V, Treluyer JM, Rey E, Jaffray P, Krivine A, Moachon L, et al. Population pharmacokinetics of tenofovir in human immunodeficiency virus-infected patients taking highly active antiretroviral therapy. Antimicrob Agents Chemother. 2005;49:3361–6.
14. Reyataz (atazanavir). [US prescribing information] Princeton: Bristol-Myers Squibb. http://packageinserts.bms.com/pi/pi_reyataz.pdf. Accessed 15th Dec 2011.
15. Elion R, Cohen C, Ward D, Ruane P, Ortiz R, Reddy YS, et al. Evaluation of efficacy, safety, pharmacokinetics, and adherence in HIV-1-infected, antiretroviral-naïve patients treated with ritonavir-boosted atazanavir plus fixed-dose tenofovir DF/emtricitabine given once daily. HIV Clin Trials. 2008;9:213–24.
16. Gallant JE, Parish MA, Keruly JC, Moore RD. Changes in renal function associated with tenofovir disoproxil fumarate treatment, compared with nucleoside reverse-transcriptase inhibitor treatment. Clin Infect Dis. 2005;40:1194–8.
17. Gallant JE, Moore RD. Renal function with use of a tenofovir-containing initial antiretroviral regimen. AIDS. 2009;23:1971–5.
18. Nishijima T, Komatsu H, Gatanaga H, Aoki T, Watanabe K, Kinai E, et al. Impact of small body weight on tenofovir-associated renal dysfunction in HIV-infected patients: a retrospective cohort study of Japanese patients. PLoS ONE. 2011;6:e22661.
19. Gerard L, Chazallon C, Taburet AM, Girard PM, Aboulker JP, Piketty C. Renal function in antiretroviral-experienced patients treated with tenofovir disoproxil fumarate associated with atazanavir/ritonavir. Antivir Ther. 2007;12:31–9.

瀬谷　司
（北海道大学）

IPS-1 Is Essential for Type III IFN Production by Hepatocytes and Dendritic Cells in Response to Hepatitis C Virus Infection

Masaaki Okamoto,* Hiroyuki Oshiumi,* Masahiro Azuma,* Nobuyuki Kato,† Misako Matsumoto,* and Tsukasa Seya*

Hepatitis C virus (HCV) is a major cause of liver disease. The innate immune system is essential for controlling HCV replication, and HCV is recognized by RIG-I and TLR3, which evoke innate immune responses through IPS-1 and TICAM-1 adaptor molecules, respectively. IL-28B is a type III IFN, and genetic polymorphisms upstream of its gene are strongly associated with the efficacy of polyethylene glycol–IFN and ribavirin therapy. As seen with type I IFNs, type III IFNs induce antiviral responses to HCV. Recent studies established the essential role of TLR3–TICAM-1 pathway in type III IFN production in response to HCV infection. Contrary to previous studies, we revealed an essential role of IPS-1 in type III IFN production in response to HCV. First, using IPS-1 knockout mice, we revealed that IPS-1 was essential for type III IFN production by mouse hepatocytes and $CD8^+$ dendritic cells (DCs) in response to cytoplasmic HCV RNA. Second, we demonstrated that type III IFN induced RIG-I but not TLR3 expression in $CD8^+$ DCs and augmented type III IFN production in response to cytoplasmic HCV RNA. Moreover, we showed that type III IFN induced cytoplasmic antiviral protein expression in DCs and hepatocytes but failed to promote DC-mediated NK cell activation or cross-priming. Our study indicated that IPS-1–dependent pathway plays a crucial role in type III IFN production by $CD8^+$ DCs and hepatocytes in response to HCV, leading to cytoplasmic antiviral protein expressions. ***The Journal of Immunology*****, 2014, 192: 2770–2777.**

Hepatitis C virus (HCV) is a major cause of chronic liver disease (1). The 3′ untranslated region (UTR) of the HCV genome is recognized by a cytoplasmic viral RNA sensor RIG-I (2). HCV RNA induces RIG-I–dependent type I IFN production to promote hepatic immune responses in vivo (2). RIG-I is a member of RIG-I–like receptors (RLRs), which include MDA5 and LGP2. RLRs trigger signal that induces type I IFN and other inflammatory cytokines through the IPS-1 adaptor molecule (3). RLRs are localized in the cytoplasm and recognize cytoplasmic dsRNAs. Another pattern recognition receptor, TLR3, recognizes dsRNAs within early endosomes or on cell surfaces (4). Human monocyte-derived dendritic cells (DCs) require TLR3 to recognize HCV RNA in vitro (5), and TLR3 induces type I IFN production through the TICAM-1 adaptor, also called Toll/IL-1R domain-containing adapter inducing IFN-β (6, 7).

*Department of Microbiology and Immunology, Hokkaido University Graduate School of Medicine, Sapporo 060-8638, Japan; and †Department of Tumor Virology, Okayama University Graduate School of Medicine, Dentistry, and Pharmaceutical Science, Okayama 700-8558, Japan

Received for publication June 3, 2013. Accepted for publication January 13, 2014.

This work was supported in part by a grant-in-aid from the Ministry of Education, Science, and Culture of Japan, the Ministry of Health, Labour, and Welfare of Japan, and the Kato Memorial Bioscience Foundation.

Address correspondence and reprint requests to Dr. Hiroyuki Oshiumi and Dr. Tsukasa Seya, Department of Microbiology and Immunology, Graduate School of Medicine, Hokkaido University, Kita-15, Nishi-7, Kita-ku Sapporo 060-8638, Japan. E-mail addresses: oshiumi@med.hokudai.ac.jp (H.O.) and seya-tu@pop.med.hokudai.ac.jp (T.S.)

The online version of this article contains supplemental material.

Abbreviations used in this article: BM-DC, bone marrow–derived dendritic cell; BM-Mf, bone marrow–derived macrophage; DC, dendritic cell; HCV, hepatitis C virus; KO, knockout; Mf, macrophage; Oc, O cured; RLR, RIG-I–like receptor; UTR, untranslated region.

Copyright © 2014 by The American Association of Immunologists, Inc. 0022-1767/14/$16.00

www.jimmunol.org/cgi/doi/10.4049/jimmunol.1301459

IL-28B is a type III IFN (also called IFN-λ), which includes IL-28A (IFN-λ2) and IL-29 (IFN-λ1) (8). Type III IFNs interacts with heterodimeric receptors that consist of IL-10Rβ and IL-28Rα subunits (8). Polymorphisms upstream of the IL-28B (IFN-λ3) gene are significantly associated with the responses to polyethylene glycol–IFN and ribavirin in patients with chronic genotype 1 HCV infections (9–12). As seen with type I IFNs, type III IFNs have antiviral activities against HCV (13). Type I IFNs induce the expression of IFN-inducible genes, which have antiviral activities, and can promote cross-priming and NK cell activation (14). However, the roles of type III IFN in cross-priming and NK cell activation are largely unknown, and the functional differences between type I and III IFN are uncertain.

Mouse $CD8^+$ DCs and its human counterpart $BDCA3^+$ DCs are the major producers of type III IFNs in response to polyI:C (15). $CD8^+$ DCs highly express TLR3 and have strong cross-priming capability (16). A recent study showed that TLR3 was important for type III IFN production by $BDCA3^+$ DCs in response to cell-cultured HCV (17). RIG-I efficiently recognizes the 3′ UTR of the HCV RNA genome, and, thus, RIG-I adaptor IPS-1 is essential for type I IFN production (2). However, the role of an IPS-1–dependent pathway in type III IFN production in vivo has been underestimated. In this study, we investigated the role of an IPS-1–dependent pathway in type III IFN production in vivo and in vitro using IPS-1 knockout (KO) mice and established an essential role of IPS-1 in type III IFN production in response to HCV RNA. Our study indicated that not only TICAM-1 but also IPS-1 are essential for type III IFN production in response to HCV.

Materials and Methods

Mice

All mice were backcrossed with C57BL/6 mice more than seven times before use. The generation of TICAM-1 and IPS-1 KO mice was described

Downloaded from http://www.jimmunol.org/ at Sapporo Ika Daigaku Fuzoku Toshokan on May 1, 2014

previously (18). All mice were maintained under specific pathogen-free conditions in the Animal Facility of the Hokkaido University Graduate School of Medicine (Sapporo, Japan). Animal experiments were conducted according to the guidelines established by the Animal Safety Center, Japan.

Cell lines and reagents

Human hepatocyte cell lines O cells and O cured (Oc) cells that contained HCV 1b replicons were provided by N. Kato (Okayama University). Mouse hepatocyte cell line was described previously (19). Poly I:C was purchased from GE Healthcare and dissolved in saline. An OVA ($H2K^b$-SL8) tetramer was purchased from MBL. PE-CD80, -CD86, -NK1.1, FITC-CD8, and allophycocyanin-CD3e Abs were purchased from BioLegend, and PE-CD40, FITC-CD69, and allophycocyanin-CD11c Abs were from eBioscience. An ELISA kit for IFN-β was purchased from PBL Biomedical Laboratories, and ELISA kits for mouse IL-28 (IFN-λ2/3) were purchased from Abcam and eBioscience. An ELISA kit for mouse IFN-γ was purchased from eBioscience. ELISA was performed according to the manufacturer's instructions. Mouse IFN-α and IFN-λ3 (IL-28B) were purchased from Miltenyi Biotec and R&D Systems, respectively.

Cell preparation

Spleen $CD8^+$ and $CD4^+$ DCs were isolated using $CD8^+$ DC isolation kit and CD4-positive isolation kit, according to manufacturer's instruction (Miltenyi Biotec). Spleen $CD11c^+$ DCs were isolated using CD11c microbeads. To obtain splenic double-negative (DN) DCs, $CD4^+$ and $CD8^+$ cells were depleted from mouse spleen cells using CD4 and CD8 MicroBeads (Miltenyi Biotec), and then $CD11c^+$ DCs were positively selected using CD11c MicroBeads (Miltenyi Biotec). We confirmed that >90% of isolated cells were $CD4^-$, $CD8^-$, and $CD11c^+$ DCs. Splenic NK cells were isolated using mouse DX5 MicroBeads (Miltenyi Biotec). The cells were analyzed by flow cytometry on a FACSCalibur instrument (BD Biosciences), followed by data analysis using FlowJo software.

Generation of bone marrow–derived DCs and bone marrow–derived macrophages

Bone marrow cells were prepared from the femur and tibia. The cells were cultured in RPMI 1640 medium with 10% FCS, 100 μM 2-ME, and 10 ng/ml murine GM-CSF or culture supernatant of L929 expressing M-CSF. Medium was changed every 2 d. Six days after isolation, cells were collected.

Hydrodynamic injection

Total RNA from the human hepatocyte cell lines O cells and Oc cells was extracted using TRIzol reagent (Invitrogen). HCV genotype 1b 3′ UTR RNA, including the polyU/UC region, was synthesized using T7 and SP6 RNA polymerase and purified with TRIzol, as described previously (20). RNA was i.v. injected into a mouse by a hydrodynamic method using a TransIT Hydrodynamic Gene Delivery System (Takara), according to the manufacturer's instruction.

Quantitative PCR

For quantitative PCR, total RNA was extracted using TRIzol reagent (Invitrogen), after which 0.1–1 μg RNA was reverse transcribed using a high-capacity cDNA transcription kit with an RNase inhibitor kit (Applied Biosystems), according to the manufacturer's instructions. Quantitative PCR was performed using a Step One real-time PCR system (Applied Biosystems). The expression of cytokine mRNA was normalized to that of β-actin mRNA, and the fold increase was determined by dividing the expressions in each sample by that of wild type at 0 h. PCR primers for mouse IFN-λ amplified both IFN-λ2 and λ3 mRNA. The primer sequences are described in Supplemental Table 1.

Activation of NK cells in vitro

NK cells and $CD11c^+$ DCs were isolated from spleens using DX5 and CD11c MicroBeads (Miltenyi Biotec), respectively. A total of 2×10^5 NK

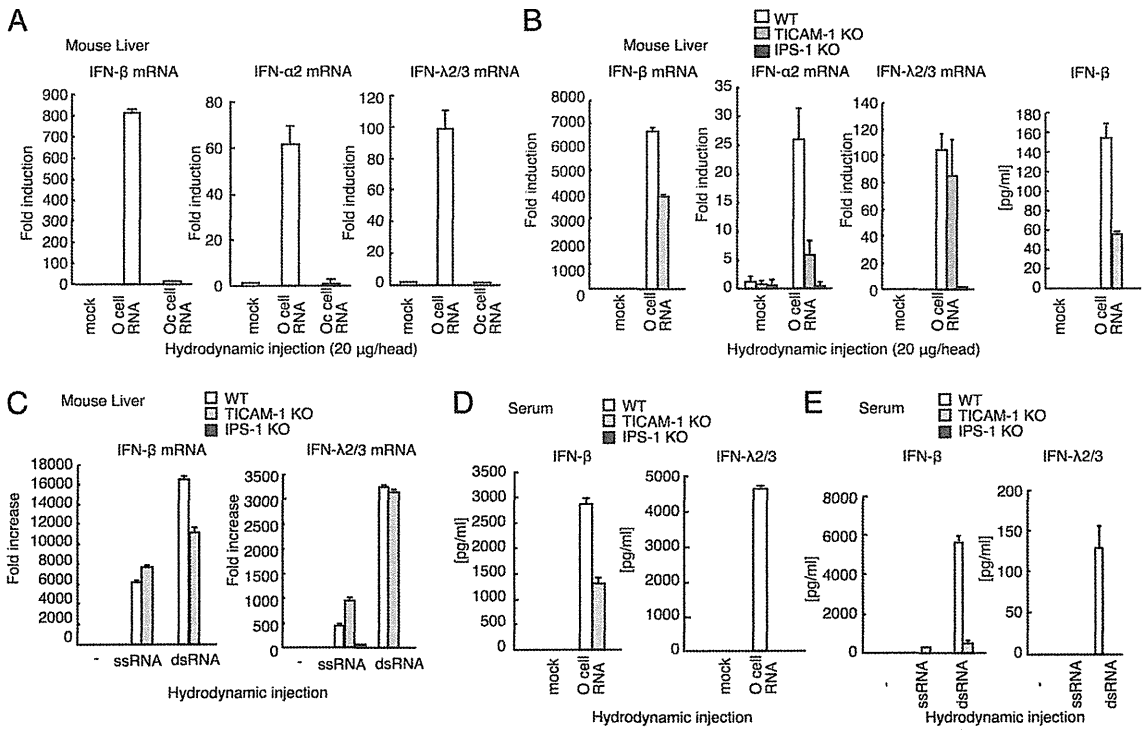

FIGURE 1. Type I and type III IFN productions in response to HCV RNA in vivo. (**A**) O cell and Oc cell RNA (20 μg) were hydrodynamically injected into wild-type mice. Six hours later, mouse livers were excised, and IFN-β, α2, and -λ2/3 mRNA levels were determined by quantitative RT-PCR. (**B**) O cell RNA (20 μg) with HCV replicons was hydrodynamically injected into wild-type, TICAM-1 KO, and IPS-1 KO mice. Six hours after injection, IFN-β, α2, and -λ2/3 mRNA levels in liver were determined by quantitative RT-PCR. IFN-β protein levels in mouse livers were determined by ELISA. (**C**) HCV ssRNA or HCV dsRNA (5 μg) was hydrodynamically injected into wild-type, TICAM-1 KO, and IPS-1 KO mice. Six hours after injection, IFN-β and -λ2/3 mRNA levels in liver were determined by quantitative RT-PCR. (**D**) O cell RNA (20 μg) with HCV replicons was hydrodynamically injected into wild-type, TICAM-1 KO, and IPS-1 KO mice. Six hours after injection, serum IFN-β and -λ2/3 concentrations were determined by ELISA. (**E**) HCV ssRNA or HCV dsRNA (5 μg) was hydrodynamically injected into wild-type, TICAM-1 KO, and IPS-1 KO mice. Six hours after injection, serum IFN-β and -λ2/3 concentrations were determined by ELISA.

Downloaded from http://www.jimmunol.org/ at Sapporo Ika Daigaku Fuzoku Toshokan on May 1, 2014

cells and 1×10^5 DCs was cocultured with IFN-λ, IFN-α, or polyI:C. After 6, 12, and 24 h, IFN-γ concentrations in the supernatants were determined by ELISA. To determine CD69 expression, $NK1.1^+$ and $CD3e^+$ cells in 24-h sample were gated.

Ag-specific T cell expansion in vivo

OVA (1 mg) and IFN-λ (0.5 μg) or 1×10^5 IU IFN-α were i.p. injected into mice on day 0, and then 0.5 μg IFN-λ or 1×10^5 IU of IFN-α was injected into mice on days 1, 2, and 4. On day 7, spleens were homogenized and stained with FITC CD8α Ab and PE-OVA tetramer for detecting OVA (SL8)-specific $CD8^+$ T cell population. For a negative control, PBS in place of IFN was injected on days 0, 1, 2, and 4. For a positive control, 100 μg polyI:C and OVA were injected into mice on day 0.

Results

TICAM-1 is essential for type III IFN production in response to polyI:C

DCs require the TLR3 adaptor TICAM-1 to produce type III IFN in response to polyI:C (15). Adding polyI:C to culture medium for mouse bone marrow–derived macrophages (BM-Mf) induced IFN-β, IFN-α2, IFN-α4, and IFN-λ2/3 mRNA expression, and TICAM-1 KO abolished IFN-λ2/3 mRNA expression (Supplemental Fig. 1A). These results suggested an essential role for TICAM-1 in type III IFN expression by BM-Mf.

Next, we examined cytokine mRNA expression in mouse tissues in response to i.p. injected polyI:C. IFN-β, IFN-α2, and IFN-α4 mRNA expression was detectable in both wild-type and TICAM-1 KO mice livers, whereas IFN-λ2/3 mRNA expression was not detected in TICAM-1 KO mouse liver (Supplemental Fig. 1B–1E). A recent study showed that TLR3 KO abolished IFN-λ serum levels in response to i.v. polyI:C injection (15). Our results and those in the previous study confirmed that TICAM-1 is essential for type III IFN expression in response to polyI:C.

IPS-1 plays a crucial role in type III IFN production in response to HCV in vivo

IPS-1 is essential for type I IFN production in response to HCV RNA and polyI:C in vivo (2, 3). We investigated whether IPS-1 could induce type III IFN production. An ectopic expression study using IPS-1 and TICAM-1 expression vectors showed that both TICAM-1 and IPS-1 activated the IFN-λ1 promoter (Supplemental Fig. 2A, 2B), which suggested that IPS-1 has the ability to induce IFN-λ1 expression. A deletion analysis showed that a 150- to 556-aa region of TICAM-1 and the transmembrane region of IPS-1 were essential for IFN-β, -λ1, and 2/3 promoter activations (Supplemental Fig. 2C, 2D).

Hydrodynamic injection is a highly efficient procedure to deliver nucleic acids to the mouse liver (21), and Gale Jr. and colleagues

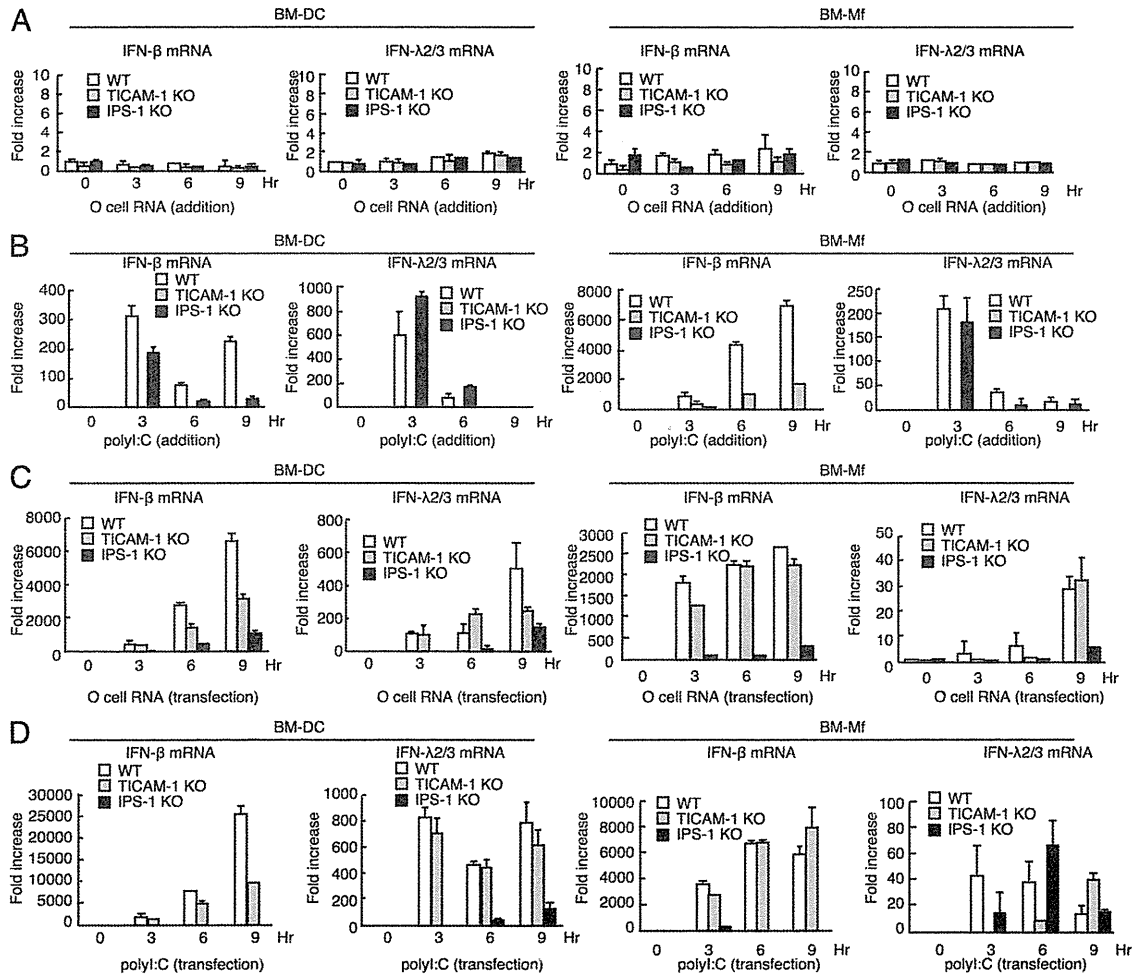

FIGURE 2. Type I and type III IFN expression in mouse DCs and Mfs in response to HCV RNA. (**A** and **B**) O cell RNA (A) or polyI:C (B) (20 μg) was added to the culture medium of BM-DCs and BM-Mfs derived from wild-type, TICAM-1 KO, and IPS-1 KO mice. IFN-β and IFN-λ2/3 mRNA levels were determined by quantitative RT-PCR at indicated hours. (**C** and **D**) O cell RNA (C) or polyI:C (D) (1 μg) was transfected into BM-DCs and BM-Mfs derived from wild-type, TICAM-1 KO, or IPS-1 KO mice. IFN-β (C) and -λ2/3 (D) mRNA levels were determined by quantitative RT-PCR.

Downloaded from http://www.jimmunol.org/ at Sapporo Ika Daigaku Fuzoku Toshokan on May 1, 2014

(2) previously used a hydrodynamic assay to assess the role of RIG-I in type I IFN production in response to HCV RNA in vivo. Thus, to investigate the response to HCV RNA in vivo, we also used a hydrodynamic assay. We used RNA extracted from hepatocyte cell lines, O cells and Oc cells. O cells are derived from HuH-7 cells and contain HCV 1b full-length replicons (22). Oc cells were obtained by eliminating these replicons using IFN-α treatment (22). RNAs extracted from O cells (with HCV RNA) and Oc cells (without HCV RNA) were hydrodynamically injected into mouse livers, after which the cytokine expressions in mouse livers were determined. In wild-type mouse liver, O cell but not Oc cell RNA induced IFN-α2, β, and λ mRNA expression (Fig. 1A), which indicated that these cytokines were expressed in response to HCV RNAs within O cells that contained the HCV genome and replication intermediates in hepatocyte. Knockout of IPS-1 severely reduced IFN-β and α2 mRNA expressions in mouse liver in response to hydrodynamically injected O cell RNA (Fig. 1B). IFN-β protein level in mouse liver was also reduced by IPS-1 knockout (Fig. 1B). Although TICAM-1 was essential for IFN-λ2/3 mRNA expression in liver in response to i.p. injected polyI:C (Supplemental Fig. 1), TICAM-1 was dispensable for IFN-λ2/3 mRNA expression in response to hydrodynamically injected O cell RNA (Fig. 1B). In contrast, IPS-1 was essential for IFN-λ2/3 mRNA expression in response to hydrodynamically injected O cell RNA (Fig. 1B). A requirement for IPS-1 for IFN-λ2/3 mRNA expression in the liver was also found when in vitro synthesized HCV dsRNAs and ssRNAs were used for the hydrodynamic assay (Fig. 1C). These results suggested that IPS-1 plays a crucial role in type III IFN production in response to HCV RNA in vivo.

To corroborate the role of IPS-1 in type III IFN production, we next measured serum IFN-λ and -β levels in response to hydrodynamic injection of O cell RNA, HCV ssRNA, and HCV dsRNA. Interestingly, IPS-1 KO markedly reduced serum IFN-λ2/3 levels (Fig. 1D, 1E). Unexpectedly, TICAM-1 KO also reduced serum IFN-λ levels (Fig. 1D, 1E). Because TICAM-1 was dispensable for IFN-λ mRNA expression in the liver, it is possible that serum IFN-λ was produced from DCs in other tissues in a TICAM-1–dependent manner, as described below. Our data indicated that both TICAM-1 and IPS-1 are essential for type III IFN in response to HCV RNA in vivo. When polyI:C was hydrodynamically injected, knockout of TICAM-1 or IPS-1 moderately reduced IFN-λ2/3 levels in sera (Supplemental Fig. 3).

DCs produce type III IFN through an IPS-1–dependent pathway in response to cytoplasmic HCV RNA

HCV proteins and minus strands of its genome are detected in DCs and macrophages (Mfs) of chronically HCV-infected patients (23, 24), and recent study showed that DCs produce type I and III IFNs in response to HCV (17, 25). Thus, we assessed the role of IPS-1 in type III IFN production by DCs and Mfs in response to HCV RNA. Surprisingly, adding O cell RNA into the culture medium did not induce any IFN-β and -λ2/3 mRNA expression (Fig. 2A), whereas adding polyI:C into culture medium efficiently induced IFN-β and -λ2/3 mRNA expression (Fig. 2B), and TICAM-1 KO abolished the IFN-λ2/3 mRNA expression in bone marrow–derived DCs (BM-DCs) and BM-Mfs (Fig. 2B). It has been shown that polyI:C is preferentially internalized and activates TLR3 in human monocyte-derived DCs, whereas in vitro transcribed viral dsRNA hardly induced IFN-β production in monocyte-derived DCs (26). Thus, there is a possibility that, unlike polyI:C, TLR3 ligand in O cell RNA was not delivered to endosome where TLR3 is localized. Next, cells were stimulated with O cell RNA or polyI:C by transfection. BM-DCs and BM-Mfs expressed IFN-β and -λ2/3

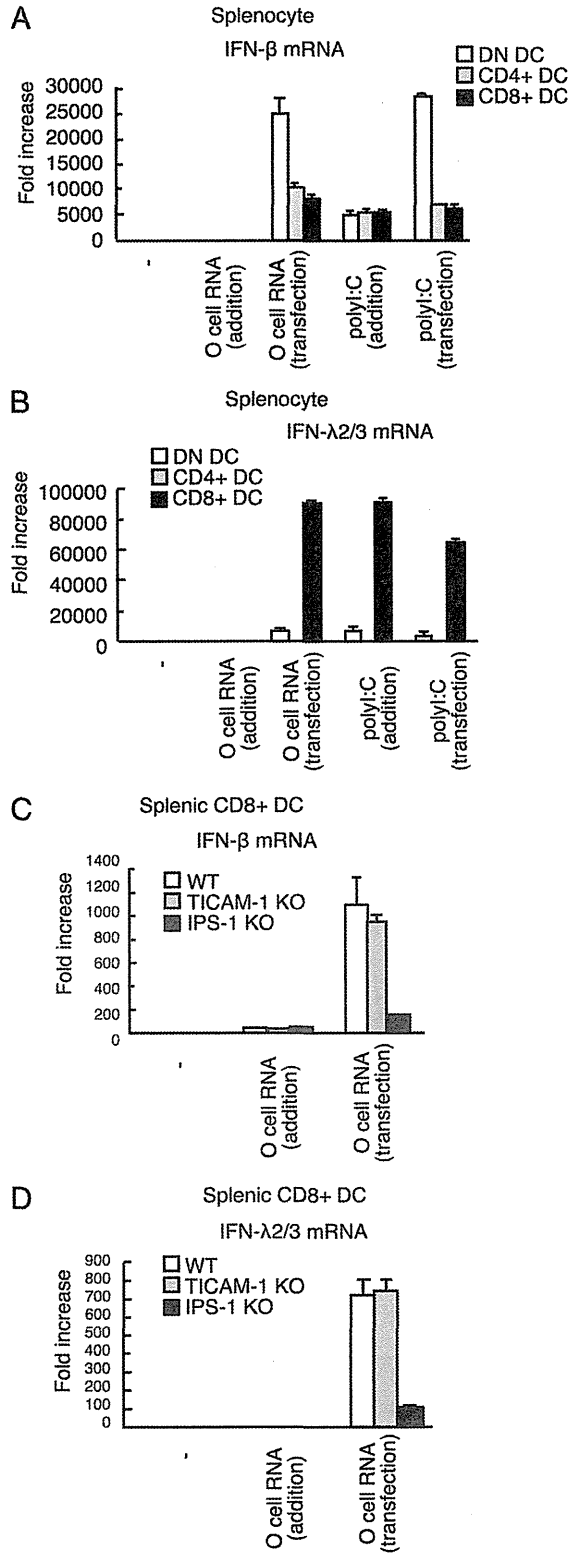

FIGURE 3. Type III IFN production by $CD8^+$ DCs. (**A** and **B**) $CD4^+$, $CD8^+$, and DN DCs were isolated from mouse spleens and stimulated with 20 μg O cell RNA without transfection or stimulated with 1 μg O cell RNA by transfection for 6 h. IFN-β (A) and -λ2/3 (B) mRNA levels were determined by quantitative RT-PCR. (**C** and **D**) $CD8^+$ DCs were isolated from wild-type, TICAM-1 KO, or IPS-1 KO mouse spleens. O cell RNA (20 μg) was added to the culture medium, or 1 μg O cell RNA was transfected into $CD8^+$ DCs. Six hours after transfection, IFN-β (C) and -λ2/3 (D) mRNA levels were determined by quantitative RT-PCR.

Downloaded from http://www.jimmunol.org/ at Sapporo Ika Daigaku Fuzoku Toshokan on May 1, 2014

mRNAs in response to O cell RNA and polyI:C (Fig. 2C, 2D). IPS-1 KO severely reduced IFN-λ2/3 mRNA expression in BM-DCs and BM-Mfs in response to O cell RNA (Fig. 2C). These results indicated that IPS-1 in BM-DCs and BM-Mfs plays a crucial role in IFN-λ2/3 mRNA expression in response to cytoplasmic HCV RNA.

Mice have $CD4^+$, $CD8^+$, and DN DCs. Thus, we next examined the IFN-β and -λ2/3 mRNA expression in these mouse DC subsets. As seen with BM-DCs, the mouse DCs expressed IFN-β and -λ2/3 mRNA in response to polyI:C but not O cell RNA in the culture medium, whereas stimulation with polyI:C or O cell RNA by transfection strongly induced their expression (Fig. 3A, 3B). Interestingly, $CD8^+$ DCs highly expressed IFN-λ2/3 mRNA in response to stimulation with polyI:C or O cell RNA by transfection compared with $CD4^+$ and DN DCs (Fig. 3A, 3B), and IPS-1 KO but not TICAM-1 KO severely reduced IFN-λ2/3 expression in $CD8^+$ DCs in response to O cell RNA transfection (Fig. 3C, 3D). This indicated that IPS-1 was essential for IFN-λ2/3 mRNA expression in $CD8^+$ DCs in response to cytoplasmic HCV RNA.

It was recently reported that exosomes mediate cell-to-cell transfer of HCV RNA from infected cells to cocultured DCs (27). We examined the production of IFN-β and -λ2/3 by $CD8^+$ DCs that were cocultured with O cells and Oc cells. Coculture with O cells but not Oc cells induced IFN-β and -λ2/3 production by $CD8^+$ DCs (Fig. 4A, 4B). Interestingly, TICAM-1 KO abolished IFN-λ2/3 mRNA expression and protein production, whereas IPS-1 KO failed to reduce IFN-λ2/3 mRNA expression and protein production in $CD8^+$ DCs (Fig. 4C, 4D). This suggested that TICAM-1 but not IPS-1 was essential for IFN-λ2/3 production by $CD8^+$ DCs when cocultured with hepatocytes with HCV replicons.

Type III IFN increases RIG-I expression in $CD8^+$ DC

The receptor for type III IFN consists of IL-10RB and IL-28Rα subunits (8). DN and $CD4^+$ DCs and NK cells did not express IL-28Rα mRNA, whereas $CD8^+$ DCs expressed both IL-10RB and IL-28Rα mRNAs (Fig. 5A). Thus, we investigated the effects of IFN-λ on DC function.

First, we examined DC cell surface markers. Unlike IFN-α, IFN-λ3 hardly increased CD40, 80, and 86 surface marker expressions on $CD8^+$ DCs (Fig. 5B). Second, we examined the effects of IFN-λ3 on cross-priming because $CD8^+$ DCs have high cross-priming capability. OVA, IFN-α, and/or IFN-λ3 were i.p. injected into mice according to the indicated schedules (Fig. 5C). Seven days after injection, OVA (SL8)-specific $CD8^+$ T cells in spleens were quantified by tetramer staining. For a positive control, OVA and polyI:C were i.p. injected into mice. The results showed that IFN-λ3 failed to increase OVA-specific $CD8^+$ T cells in the spleens and suggested that IFN-λ3 failed to promote cross-priming at least in our experimental condition (Fig. 5C).

Third, we examined NK cell activation by DCs. NK cells and DCs were isolated from mouse spleens and were cocultured for 24 h in the presence of IFN-α, λ3, or polyI:C. Although IFN-γ production was increased by IFN-α stimulation, IFN-λ3 failed to increase IFN-γ production (Fig. 5D). Next, we investigated a cell surface marker for NK cells when cocultured with DCs. The expression of CD69, a NK cell activation marker, was not increased by IFN-λ3 stimulation (Fig. 5E). These results indicated that, unlike IFN-α, IFN-λ3 failed to enhance the activation of NK cells by DCs.

Fourth, we investigated the expression of antiviral genes in $CD8^+$ DCs in response to IFN-λ3 stimulation. Interestingly, IFN-λ3 stimulation increased RIG-I and Mx1 but not TLR3 mRNA expression in $CD8^+$ DCs (Fig. 6A). In addition, pretreatment with IFN-λ3 augmented IFN-λ2/3 mRNA expression in $CD8^+$ DCs in response to HCV RNA (Fig. 6B). Taken together, type III IFN induced RIG-I and antiviral protein expression but failed to promote DC-mediated NK cell activation and cross-priming.

Hepatocytes express type III IFN receptors. Thus, we examined the effects of IFN-λ on mouse hepatocytes. As with IFN-α, IFN-λ3 stimulation induced both TLR3 and RIG-I mRNA expression in mouse hepatocyte (Fig. 6C). Antiviral nucleases, ISG20 and RNaseL, and an IFN-inducible gene, Mx1, were induced by IFN-λ3 or IFN-α treatment (Fig. 6C). Pretreating mouse hepatocytes with IFN-λ3 enhanced IFN-β and -λ2/3 mRNA expression in response to stimulation with HCV RNA by transfection (Fig. 6D). These results indicated that IFN-λ3 induced cytoplasmic antivirus protein expression in mouse hepatocytes. We confirmed that IFN-λ3 treatment significantly reduced HCV RNA levels in O cells with HCV replicons (Fig. 6E). A previous study also reported that IFN-λ inhibits HCV replication (13).

Discussion

Previous studies have established the importance of the TLR3 pathway for type III IFN production in response to polyI:C (15) or HCV (17). In this study, we established the importance of IPS-1–dependent pathway for type III IFN production in response to cytoplasmic HCV RNA in vivo and in vitro using a mouse model. These data indicated that there are at least two main pathways for type III IFN production in vivo, as follows: one is TICAM-1 dependent, and the other is IPS-1 dependent.

We revealed that IFN-λ was efficiently produced by $CD8^+$ DCs, the mouse counterpart of human $BDCA3^+$ DCs, in response to

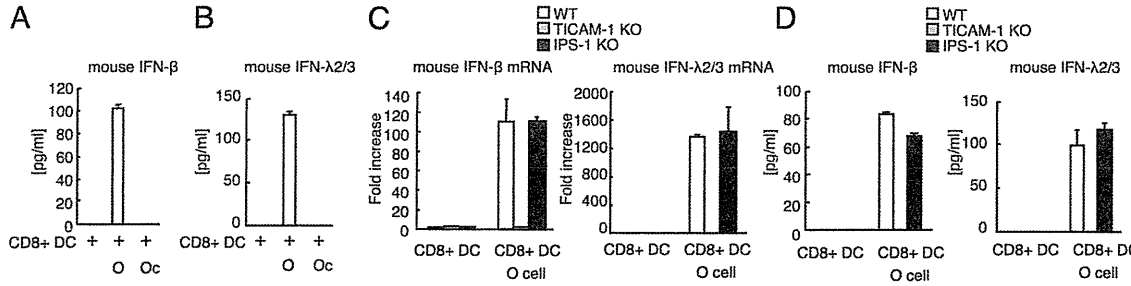

FIGURE 4. IFN-β and –λ production by $CD8^+$ DCs cocultured with hepatocytes with HCV replicons. (**A** and **B**) $CD8^+$ DCs isolated from wild-type spleens were cocultured with O cells (with HCV replicons) or Oc cells (without HCV replicons). After 24 h of coculture, IFN-β (A) and –λ2/3 (B) concentrations in culture medium were determined by ELISA. (**C**) $CD8^+$ DCs isolated from wild-type, TICAM-1 KO, or IPS-1 KO spleens were cocultured with O cells with HCV replicons for six hours, and then IFN-β and –λ2/3 mRNA expression was determined by RT-qPCR. (**D**) $CD8^+$ DCs isolated from wild-type, TICAM-1 KO, or IPS-1 KO spleens were cocultured with O cells with HCV replicons. IFN-β and –λ2/3 concentrations in culture medium were determined by ELISA.

Downloaded from http://www.jimmunol.org/ at Sapporo Ika Daigaku Fuzoku Toshokan on May 1, 2014

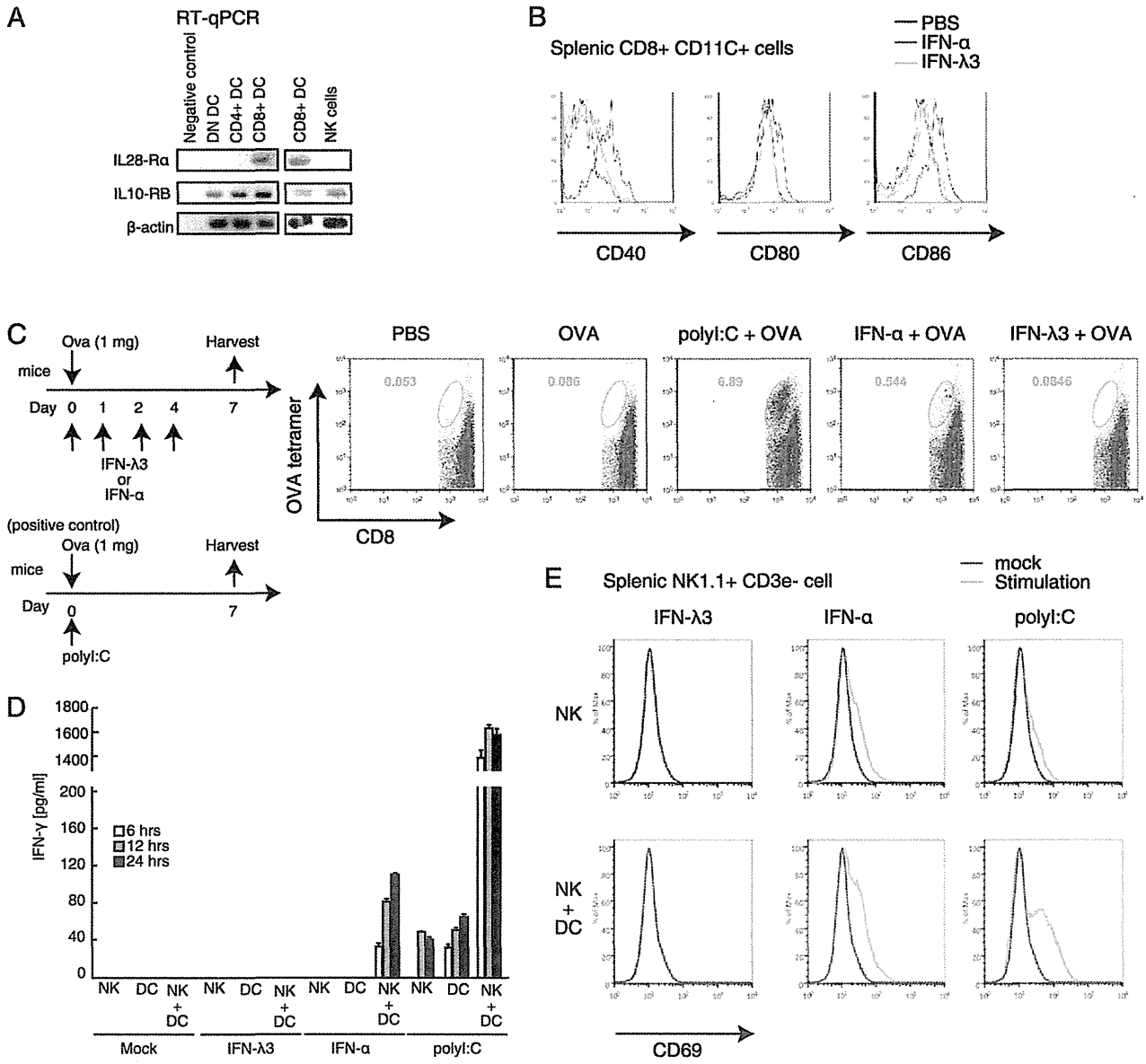

FIGURE 5. IFN-λ effects on DC functions. (**A**) DN, $CD4^+$, $CD8^+$ DCs, and NK cells were isolated from wild-type mouse spleens. IL-28Rα and IL-10RB mRNA were determined by RT-PCR. (**B**) A total of 0.5 μg IFN-λ3 or 1×10^5 IU IFN-α was i.p. injected into mice. Six hours after injection, spleen $CD8^+$ DCs were isolated, and cell surface expressions of CD40, 80, and 86 were determined by FACS analysis. (**C**) OVA and IFN-λ or IFN-α were i.p. injected into mice on day 0, and then IFN-λ or IFN-α was injected into mice on days 1, 2, and 4. Spleens were excised on day 7, and OVA (SL8)-specific $CD8^+$ T cells were determined by a tetramer assay. For a negative control, PBS in place of IFN was injected on days 0, 1, 2, and 4. For a positive control, polyI:C and OVA were injected into mice on day 0. (**D**) NK cells and $CD11c^+$ DCs were isolated from mouse spleens and then stimulated with 1000 U/ml IFN-α, 100 ng/ml IFN-λ3, or 100 μg/ml polyI:C. IFN-γ concentrations in the culture medium at the indicated times were determined by ELISA. (**E**) NK cells were isolated from mouse spleens and then cultured with or without spleen $CD11c^+$ DCs. Cells were stimulated with 1000 U/ml IFN-α, 100 ng/ml IFN-λ3, or 20 μg polyI:C. CD69 expression on NK cells was determined by FACS analysis.

cytoplasmic HCV RNA. Moreover, our data showed that IFN-λ stimulation increased the mRNA expression of RIG-I but not that of TLR3 in $CD8^+$ DCs, and $CD8^+$ DCs required IPS-1 to produce IFN-λ in response to stimulation with cytoplasmic HCV RNA. Furthermore, IFN-λ enhanced the mRNA expression of IFN-λ itself in $CD8^+$ DCs, which suggested a positive feedback loop for IFN-λ mRNA expression in $CD8^+$ DCs. IFN-λ failed to promote DC-mediated NK activation or cross-priming at least in our experimental conditions, whereas antiviral proteins, such as ISG20 and RNaseL, were efficiently induced by IFN-λ stimulation in hepatocytes and $CD8^+$ DCs. These results established a novel role of IPS-1 in innate immune response against HCV via IFN-λ production. IFN-λ pretreatment markedly increased IFN-β mRNA expression in response to HCV RNAs in mouse hepatocyte but not in $CD8^+$ DCs (Fig. 6B, 6D). Although the underlying mechanism is unclear, it is possible that there is a cell-type–specific role of IFN-λ.

It was recently reported that $BDCA3^+$ DCs require TLR3 for type III IFN production in response to cell-cultured HCV (17). They used a HCV 2a JFH1 strain that cannot infect human DCs in vitro (5). We also showed that the TLR3 adaptor TICAM-1 was essential for type III IFN production by $CD8^+$ DCs when cocultured with O cells with HCV replicons. Thus, TLR3 appears to be essential for type III IFN production by DCs that are not infected with HCV. It

Downloaded from http://www.jimmunol.org/ at Sapporo Ika Daigaku Fuzoku Toshokan on May 1, 2014